Chinese Herbal Medicines 16 (2024) 638–655

Contents lists available at ScienceDirect

Chinese Herbal Medicines

journal homepage: www.elsevier.com/locate/chmed

Original Article

Network pharmacology, molecular docking, and untargeted metabolomics reveal molecular mechanisms of multi-targets effects of Qingfei Tongluo Plaster improving respiratory syncytial virus pneumonia

Mengfei Yang [a], Xiuying Zhang [b,*], Qing Liu [a], Yongxue Wang [a]

[a] Graduate School, Liaoning University of Traditional Chinese Medicine, Shenyang 110032, China
[b] Department of Pediatrics, Affiliated Hospital of Liaoning University of Traditional Chinese Medicine, Shenyang 110847, China

ARTICLE INFO

Article history:
Received 16 August 2023
Revised 20 February 2024
Accepted 26 July 2024
Available online 29 July 2024

Keywords:
children
metabolomics
network pharmacology
PIK3/AKT pathway
Qingfei Tongluo Plaster
respiratory syncytial virus pneumonia

ABSTRACT

Objective: Qingfei Tongluo Plaster (QFP), an improved Chinese medicine hospital preparation, is an attractive treatment option due to its well clinical efficacy, convenience, economy, and patient compliance in the treatment of respiratory syncytial virus (RSV) pneumonia. The aim of this study was to investigate the efficacy mechanism of QFP on RSV rats from the perspective of alleviating lung inflammation and further explore the changes of serum metabolites and metabolic pathways in RSV rats under the influence of QFP.

Methods: This study used network pharmacological methods and molecular docking combined with molecular biology and metabolomics from multi-dimensional perspectives to screen and verify the therapeutic targets. Open online databases were used to speculate the gene targets of efficient ingredients and diseases. Then, we used the String database to examine the fundamental interaction of common targets of drugs and diseases. An online enrichment analysis was performed to predict the functional pathways. Molecular docking was applied to discover the binding modes between essential ingredients and crucial gene targets. Finally, we demonstrated the anti-inflammatory ability of QFP in the RSV-evoked pneumonia rat model and explained the mechanism in combination with the metabolomics results.

Results: There were 19 critical targets defined as the core targets: tumor necrosis factor (*TNF*), inducible nitric oxide synthase 2 (*NOS2*), mitogen-activated protein kinase 14 (*MAPK14*), g1/S-specific cyclin-D1 (*CCND1*), signal transducer and activator of transcription 1-alpha/beta (*STAT1*), proto-oncogene tyrosine-protein kinase Src (*SRC*), cellular tumor antigen p53 (*TP53*), interleukin-6 (*IL6*), hypoxia-inducible factor 1-alpha (*HIF1A*), RAC-alpha serine/threonine-protein kinase (*AKT1*), signal transducer and activator of transcription 3 (*STAT3*), heat shock protein HSP 90-alpha (*HSP90AA1*), tyrosine-protein kinase JAK2 (*JAK2*), cyclin-dependent kinase inhibitor 1 (*CDKN1A*), mitogen-activated protein kinase 3 (*MAPK3*), epidermal growth factor receptor (*EGFR*), myc proto-oncogene protein (*MYC*), protein c-Fos (*FOS*) and transcription factor p65 (*RELA*). QFP treated RSV pneumonia mainly through the phosphatidylinositol 3-kinase (PI3K)/RAC AKT pathway, HIF-1 pathway, IL-17 pathway, TNF pathway, and MAPK pathway. Animal experiments proved that QFP could effectively ameliorate RSV-induced pulmonary inflammation. A total of 28 metabolites underwent significant changes in the QFP treatment, and there are four metabolic pathways consistent with the KEGG pathway analyzed by network pharmacology, suggesting that they may be critical processes related to treatment.

Conclusion: These results provide essential perspicacity into the mechanisms of action of QFP as a promising anti-RSV drug.

1. Introduction

Among children's respiratory tract infections, respiratory syncytial virus (RSV) is the most common cause, with increased susceptibility in those before the age of two years (Nair et al., 2010). Respiratory syncytial virus pneumonia (RSVP) accounts for 22% of children's acute lower respiratory tract infections worldwide. A European prospective cohort study involving 993 healthy term-born infants showed that approximately 1.79% of infants required hospitalization following RSVP infections in high-income settings, which imposes a heavy financial burden on healthcare systems

* Corresponding author.
E-mail address: 1370264413@qq.com (X. Zhang).

https://doi.org/10.1016/j.chmed.2024.07.007
1674-6384/

(Wildenbeest et al., 2022). RSV children may develop asthma and wheezing due to future long-term respiratory problems if they suffer severe symptoms from the infection (Punnoose & Golub, 2012). In underdeveloped countries and regions, RSV is a significant cause of death. A decrease in RSV infections was notable at the beginning of the Coronavirus Disease 2019 (COVID-19) pandemic (Chow, Uyeki, & Chu, 2022). However, the increase in RSV cases was more prominent than in previous years as nonpharmaceutical interventions (NPIs) were lifted (Britton et al., 2020; Ujiie, Tsuzuki, Nakamoto, & Iwamoto, 2021), which attributed to the reductions of population-level immunity and re-engagement in public activities of children (Chow, Uyeki, & Chu, 2022). Previous studies have found that Ribavirin, a broad-spectrum antiviral, is not recommended in routine due to its toxicity and side effects (Ventre & Randolph, 2007). Simultaneously, as an anti-RSV vaccine, Palivizumab is administered mainly to high-risk children, including premature infants and those with a history of heart, lung, or neuromuscular disease, and is not a correct recommendation for the general patient. The high price further restricts its market circulation (Jain, Schweitzer, & Justice, 2023). Hence, comprehending host-virus fundamental interactions that govern RSV's ability to affect the immunologic response is crucial for developing beneficial remedial and preventive strategies.

The mechanism of RSVP in the traditional Chinese medicine (TCM) system is "lung heat and stagnation of lung *qi*". Qingfei Tongluo Plaster (QFP), adapted from the "Dachengqi Decoction" in *Treatise on Febrile Diseases*, composed of the alcohol extract of traditional medicine *Rhei Radix* et *Rhizoma* (Dahuang in Chinese, DH) and *Scutellariae Radix* (Huangqin in Chinese, HQ). In ancient times, Dachengqi Decoction was used for the treatment of pulmonary diseases with "lung heat and stagnation of lung *qi*" syndromes based on the theory of "the lung and the large intestine being interior-exteriorly related" and the method of "tongfu-dispelling heat therapy" (Zeng, 2014). Considering the resistance to oral medication and the fear of intravenous infusion in children, we adapted the decoction into QFP, a plaster applied directly to the "Feishu" or areas with dense pulmonary rales that can improve patient compliance (Zhang et al., 2017). Transdermal administration, allowing the drug to constantly pass through the layers of skin or mucous membranes to treat disease, avoids the first-pass effect to maintain a stable blood concentration, reducing liver and kidney toxicity and intestinal flora disorder. Moreover, through the stimulation of acupoints and meridians by drugs, the function of the meridian system is stimulated, and the body's *yin*, *yang*, *qi*, and *blood* are corrected. Due to the characteristics of convenience and economy, QFP has been widely used in the pediatric department in our hospital. Previous studies have demonstrated that QFP could regulate T helper 1/T helper 2 (Th1/Th2) imbalance, reduce viral load, and inhibit the activation of the mitogen-activated protein kinase (MAPK) pathway in RSVP rats (Zhang, Wang, Liu, & Wang, 2016; Zhang, Wang, & Song, 2016; Zhang, Wang, & Yan, 2017). Our randomized controlled trial covering 689 children with pneumonia showed that QFP could shorten the duration of fever, sputum production, wheezing, and pulmonary rales by promoting the absorption of inflammation to improve recovery rates (Wei et al., 2013; Zhang et al., 2017). The previous research of our group has shown that the active ingredients in QFP, such as emodin, rhein and baicalin, could penetrate the skin, and the extraction process of QFP is stable, reasonable and feasible, which can be used for promotion and production (Zhang, 2016). However, we still need to comprehensively understand the therapeutic mechanism of QFP in treating RSVP. For example, what active ingredients play a central therapeutic role in the two QFP drugs? What are the core targets and pathways of QFP treatment in RSVP rats? What potential biomarkers and metabolic pathways are the focus of QFP interventions?

Based on the balance-regulation theory, TCM emphasizes adjusting the human body's integrity. However, research on its pharmacological mechanism is challenging due to the complex character of TCM (Zhou & Feng, 2023). Our study constructed the "compound-gene target-pathway" network using experimental methods such as network pharmacological analysis, molecular docking, molecular biology, and metabolomics techniques. An overview of metabolomics focuses on organs or tissues, their interactions with external and internal factors, and the metabolic pathways by which these endogenous metabolites are transported. Combining metabolomics with online data analysis can reveal further molecular mechanisms of disease progression.

2. Materials and methods

2.1. Reagents and instruments

Agilent 1290 infinity UPLC liquid chromatograph was from Agilent (Santa Clara, USA); Triple TOF 5600 + mass spectrometer was obtained from AB SCIEX (Boston, USA); ACQUITY UPLC BEH amide 100 mm × 2.1 mm, 1.7 μm column was obtained from Waters (Milford, Ireland); Acetonitrile was purchased from Merck (batch No.: 1499230-935, Darmstadt, Germany); Ammonium acetate was from Sigma (batch No.: 70221, St. Louis, USA); Methanol was from Merck (batch No.: 144282, Darmstadt, Germany); Ammonia was purchased from Merck (batch No.: 105426, Darmstadt, Germany); Rat interleukin-6 (IL-6) elisa kit was from Signalway Antibody (SAB) (batch No.: EK0519, Maryland, USA); Radio immunoprecipitation assay (RIPA) lysis buffer was purchased from Beyotime (batch No.: P0013B, Shanghai, China); Bicinchoninic acid (BCA) protein concentration assay kit was obtained from Beyotime (batch No.: P0009, Shanghai, China); Polyvinylidene fluoride (PVDF) membrane was from Millipore (batch No.: IPVH00010, Billerica, USA); Phosphatidylinositol 3-kinase (PI3K) P85 antibody was from Proteintech Group, Inc (batch No.: 60225-1-Ig, Wuhan, China); p-PI3K P85 antibody was obtained from abclonal (batch No.: AP0854, Woburn, USA); Threonine-protein kinase (AKT) antibody was from Cell Signaling Technology (CST) (batch No.: 9272, Danvers, USA); p-AKT antibody was obtained from CST (batch No.: 9271S, Danvers, USA); Hypoxia-inducible factor-1alpha (HIF-1α) antibody was purchased from Cusabio (batch No.: CSB-PA000432, Houston, USA); Inducible nitric oxide synthase 2 (NOS2) antibody was from Cusabio (batch No.: CSB-PA003464, Houston, USA); Beta-actin (β-actin) was from purchased Abcam (batch No.: ab8227, Cambridge, USA); Goat Anti-Rabbit IgG-Horseradish peroxidase (Goat Anti-Rabbit IgG-HRP) was obtained from Thermo Fisher Scientific (batch No.: 31460, Waltham, USA).

2.2. Network pharmacological study

2.2.1. Potential ingredient inspection

Through searching the Traditional Chinese Medicine Systems Pharmacology Database (TCMSP) (Ru et al., 2014) and reassessing the pertinent literatures, potential compounds in QFP (*Rhei Radix* et *Rhizoma* and *Scutellariae Radix*) were detected. Searching for active compounds based on oral bioavailability (OB) and drug-like properties (DL) cannot be used to predict transdermal mechanisms. In order to better elucidate QFP's activity concerning transdermal absorption components, we referenced the screening threshold of predicting transdermal drug delivery (Naik, Kalia, & Guy, 2000) and Lipinski's rules of five (Alamri et al., 2021) to establish a correlation between the two. The values were molecule weight < 500 g/mol, 1 < Log*P* < 3, rotatable bonds < 10, hydrogen bond donors < 5, and hydrogen bond acceptors < 10. All ingredients

were screened through the SwissADME online platform (Daina, Michielin, & Zoete, 2017).

2.2.2. Prediction of targets for QFP ingredients

TCMSP and Swiss Target Prediction (Daina, Michielin, & Zoete, 2019) were employed to predict the gene targets of QFP, and the corresponding targets of QFP were collected. The PubChem Cid number of each active ingredient was obtained using TCMSP, and we updated potential targets via Swiss Target Prediction regarding the SMILE codes, or 2D images of compounds generated from PubChem (Kim et al., 2019) in SDF format were used to update potential targets via Swiss Target Prediction. Our research assigned a probability value of $\geq$ 0.1 to screen out protein targets and exclude the repetition after collecting the targets of TCMSP. Eventually, we built the "QFP-compound-target" network with Cytoscape 3.9.1 software (Shannon et al., 2003) after the official annotation of the potential targets on the UniProt database (Consortium, 2023).

2.2.3. Acquisition of RSVP targets

Choosing "respiratory syncytial virus pneumonia" as the passphrase, we inspected the OMIM database (Kui et al., 2021), GeneCards database (Stelzer et al., 2016), and Drugbank database (Wishart et al., 2018) to recognize the target genes appertained to RSVP. Furthermore, We searched "("respiratory syncytial viruses"[MeSH Terms] OR "respiratory syncytial virus"[Organism] OR ("respiratory syncytial viruses"[MeSH Terms] OR "respiratory syncytial virus"[Organism] OR respiratory syncytial virus[All Fields]))" AND "Homo sapiens"[porgn] AND ("tissues"[MeSH Terms] OR normal[All Fields]) AND "gse"[Filter] in the Gene Expression Omnibus (GEO) DataSets (Edgar, Domrachev, & Lash, 2002), stipulated humans as the species. All disease-related datasets were retrieved, and the content and source of samples were viewed individually. Normal control, measured mRNA, and human source samples were required to be included. Regarding GEO analysis, $|\log_2(\text{fold change})| > 1$ and P-value < 0.05 were the circumstances for RSVP-related greatly differential expression genes. The bioinformatics online platform plotted the volcano plot for data analysis and visualization (Bioinformatics, 2021). Eventually, the online Venn mapping website mapped the common targets of QFP and RSVP (Bardou, Mariette, Escudié, Djemiel, & Klopp, 2014). Obvolute proteins were then regarded as immanent therapeutical targets for the intervention of RSVP.

2.2.4. Protein-protein interaction (PPI) network construction

We built a PPI network after importing the common targets of "QFP-RSVP" into the search tool for recurring instances of neighbouring genes (STRING) (Szklarczyk et al., 2021) to further study the role of crucial targets. In our study, the minimum demanding interrelation score was chosen in the highest confidence score ($\geq$ 0.900) with the 'Homo sapiens', and the unconnected nodes were concealed. The interaction network was represented by Cytoscape 3.9.1. The CytoNCA (Cytoscape software add-in) (Tang, Li, Wang, Pan, & Wu, 2015) was installed to analyze the topological characteristics of the targets. By utilizing the PPI network, key targets were identified based on degree value (Degree), closeness centrality (CC), and betweenness centrality (BC).

2.2.5. Gene ontology (GO) and kyoto encyclopedia of genes and genomes (KEGG) pathway enrichment analyses

To further clarify the gene occupation of QFP and the role of intrinsic signaling pathways in RSVP, GO and KEGG pathway assessments of 131 target genes were accomplished using Metascape (Zhou et al., 2019). The bioinformatics platform plotted the bar with bar with a color gradient for data analysis and visualization. We used the FDR error control technique to determine whether biological processes differed significantly. The P-value was corrected, and a threshold value of $P < 0.05$ was scored for significance.

2.2.6. Molecular docking processing

We used computer-assisted technology in this study to confirm further the intensity of the interaction between the targets and core compound. The molecular structures of core protein targets were acquired from the Protein Data Bank (PDB) database (Burley et al., 2021), and the mol2 files of the structures of ingredients were obtained from the TCMSP. The original ligands and water molecules of proteins were removed by PyMOL software (Schrödinger & DeLano, 2020). To select the best conformation from docking simulations, small molecules were pre-processed using the AutoDock 4.2 software (Morris et al., 2009). Using binding free energy, all molecules and disease targets were ranked by their interaction strength after docking simulations. The docking was recognized as valid when the binding free energy was under −20.92 kJ/mol. Finally, the highest binding energy component in each target was visualized by PyMOL software, and we used GraphPad Prism 8.0.2 (GraphPad, CA, USA) to draw a heatmap of the binding energy.

2.3. Experimental verification

2.3.1. QFP preparation

Traditional Chinese medicine was acquired from the dispensary of the First Affiliated Hospital of Liaoning University of Traditional Chinese Medicine. The extraction process was determined following our previous research, and we continued quality control and *in vitro* transdermal absorption experiments, which proved that the effective material basis for QFP can enter the blood circulation through the skin and play a therapeutic role (Fig. S1 and Table S1) (Zhang, 2016). 40 g of *Rhei Radix* et *Rhizoma* (batch No.: 2206063) and *Scutellariae Radix* (batch No.: 2207011) were weighed and placed in a 1 000 mL volumetric flask. Six times the amount of 70% ethanol was added and heated for reflux extraction three times, 1 h for each extraction. The extract was filtered and merged, and the ethanol was recovered until it had no alcohol flavor. Then, it was dried in a drying baker until the weight was constant. After completely drying, grinding it into a powder and storing it in a cool, dry place. It was mixed with minced garlic when using and prepared freshly.

2.3.2. RSV production

The RSV-long strain originated from the Capital Institute of Pediatrics, and the human epithelioma-2 (HEp-2) cell line was purchased from the Virology Institute of the Chinese Academy of Preventive Medicine, which were both cryopreserved in the Virus Laboratory of the Affiliated Hospital of Liaoning University of Traditional Chinese Medicine. The virus was amplified in HEp-2 cells and quantified by detecting the 50% tissue culture infective dose (TCID50), similar to our prior study (Wang, 2015; Zhang, 2016). The phosphate buffer saline (PBS) was used to dilute the virus stock solution.

2.3.3. Animal administration

A total of 21 male SD rats (weight range 50−70 g) were obtained from Liaoning Changsheng Biotechnology Co., Ltd. (Grant number: SYXK 2020-0001). The experimental animal center of Liaoning University of Traditional Chinese Medicine provided rats free access to food and water in a pathogen-free environment at 25 °C. Licensed experiments with animals were approved by the Animal Care & Welfare Committee of Liaoning University of Traditional Chinese Medicine (Grant number: 21000042022038).

Three groups of rats were randomly divided after 3 d of adaptive feeding (n = 6 in each group). (1) Normal group (Nor), (2)

model group (Mod), and (3) QFP group. The model group and the QFP group were challenged intranasally (i.n.) with 10 TCID50 (10^{-3}) viral stock (100 μL) under inhaled isoflurane anesthesia for three consecutive days. The normal group was infected with the same amount of vehicle (PBS). A 3 cm × 4 cm area of the back hair was briefly shaved off to expose the skin entirely. The amount of raw herbs contained in the plaster used was 10.5 g/kg (Hao, Wang, Liu, Shao, & Xie, 2016). The QFP was spread evenly on the gauze (the thickness of one coin) and was attached to the back of the rat from the QFP group for 30 min once a day for five consecutive days after modeling. As a control, the other rats were smeared with the same amount of saline in the same place for the same duration.

2.3.4. Enzyme-linked immunosorbent assay (ELISA)

After successful anesthesia with isoflurane 5 d post-infection, vacuum catheters were used to collect abdominal aortic blood. Whole blood was centrifuged for 10 min at 3 000 g/min at room temperature after being set for 4 h. Then, the serum was separated, and the measurements of IL-6 levels were performed according to the ELISA kit instructions.

2.3.5. Determination of lung index

Weighing after lung removal and lung index was calculated by the equation:

$$\text{Lung index (\%)} = \text{lung wet weight (g)/body weight (g)} \times 100.$$

2.3.6. Hematoxylin eosin (HE) staining

The lungs fixed with 4% paraformaldehyde were imbedded into wax blocks and sliced into slices of about 5 μm by a microtome (three sections from each lung, six lungs per group). The light microscope was used to observe the pulmonary histopathology after HE staining. Images were collected by a high-definition OlympusBX50 biological microscope and analyzed according to the scoring method (Belperio et al., 2002), and then a mean ± SD was calculated for the cumulative values.

2.3.7. Protein immunoblot

The RIPA lysate was used to extract all proteins from rat lungs, and the BCA reaction was used to estimate the concentrations. After sodium dodecyl sulfate polyacrylamide gel electrophoresis (SDS-PAGE), the samples were transferred to the PVDF membrane. After blockading with 5% (M/V) skim milk powder equipped with tris buffered saline with tween® 20 (TBST), the following primary antibodies were incubated: PI3K P85 (1:1 000), p-PI3K P85 (1:1 000), AKT (1:1 000), p-AKT (1:1 000), HIF-1α (1:1 000), NOS2 (1:1 000), and β-actin (1:1 000). Goat Anti-Rabbit IgG-HRP (1:8 000) was incubated for 1 h on the membranes at room temperature. β-actin was applied for standardization. Every protein band was measured for its sum density on the WD-9413B gel imaging system (Beijing Liuyi Biotechnology Co., Ltd., Beijing, China).

2.3.8. Data analysis

The mean ± standard deviation (SD) represented the statistical information, and $P < 0.05$ was considered significantly different. T-tests were applied when the distributions of the two groups were normal, and the variance was homogenous. One-way analysis of variance (ANOVA) was used for multi-group comparison. Finally, figures were drawn using GraphPad Prism 8.0.2.

2.4. Serum metabolomics research

2.4.1. Sample preparation

Serum (100 μL) was mixed with 400 μL methanol acetonitrile with vortex and was centrifuged at 14 000 × *g* for 20 min at 4 °C after being processed with sonication in ice baths. The supernatants were dried by liquid chromatograph-mass spectrometer (LC-MS) analysis. In addition, quality control (QC) samples were used for data normalization to guarantee the data quality of metabolic analysis. The preparation and analysis processes of QC samples were the same as that of each batch of experimental samples.

2.4.2. Ultra-high performance liquid chromatography with quadrupole time-of-flight mass spectrometry (UPLC-Q-TOF-MS) analysis

UPLC-ESI-Q-TOF-MS system combined with TripleTOF 5600 was used to analyze the metabolomics profiling. Samples were analyzed using the ACQUITY UPLC BEH Amide 100 mm × 2.1 mm, 1.7 μm column. Using 25 mmol/L ammonium acetate, 25 mmol/L ammonium hydroxide (A)-100% acetonitrile (B) at a flowing rate of 0.5 mL/min by a gradient elution: 0.5 min, 95% B; 6.5 min, 65% B; 2 min, 40% B; 6.1 min, 95% B. In positive and negative modes, MS data acquisition was analyzed by electrospray ionization (ESI). Source conditions for ESI were: 60 ion source gas 1, 60 ion source gas 2, 30 curtain gas, 600 °C source temperature, ± 5 500 V ionspray voltage floating (ISVF) in the source. MS-only acquisitions were set to target *m*/*z* 60−1 200, with a TOF MS accumulation time of 0.15 s/spectra. Auto MS/MS acquisition was set to acquire across the *m*/*z* range 25−1 200, with a maintenance accumulation time of 0.03 s/spectra. The collisional energy was set as 30 V ± 15 eV, and declustering potential was fixed at ± 60 V. Every six samples during acquisition, QC and blank samples (75% acetonitrile in water) were injected.

2.4.3. Data preprocessing and filtering, multivariate statistical analysis and pathway analysis

All multivariate data analyses and modeling were performed by SIMCAP software (Version 14.0, Umetrics, Umeå, Sweden). Principal component analysis (PCA), partial least square discriminant analysis (PLS-DA), and orthogonal partial least square discriminant analysis (OPLS-DA) were used to generate models. With permutation tests, we evaluated all the models for overfitting. OPLS-DA allowed the determination of discriminating metabolites using the variable importance on projection (VIP). At the univariate analysis level, we obtained the discriminating metabolites from a threshold of variable influence on projection values calculated from the two-tailed Student's *t*-test (*P-value*) and OPLS-DA model. Multiple group analysis was calculated using a ANOVA. The statistical significance of metabolites was determined by VIP-value > 1.0 and *P*-value < 0.05. The fold change calculation was based on the ratio of two arbitrary mass responses (areas). Furthermore, cluster analyses were performed using the R package on the identified differential metabolites. Pathway analysis of potential biomarkers was performed with MetaboAnalyst 5.0 (MetaboAnalyst, 2009). After screening out the common metabolic and KEGG pathways, the network diagram was drawn by Cytoscape 3.9.1.

3. Results

3.1. Screening of ingredients and selection of gene targets

A total of 135 components were collected by searching the literature and online platforms, and 42 qualified ingredients were selected through our screening threshold. Ingredient structures were obtained in the TCMSP database, and Table 1 represents details of active ingredients. A total of 2 999 QFP targets were identified based on the online databases. The results showed that 398 genes were identified by deleting the duplicate and unreviewed genes using the PubChem database. The "chemical composition-target" network of QFP was built using Cytoscape 3.9.1, showing the connection between 42 components and 398 target genes

Table 1
Information of active ingredients.

No.	Drugs	Family	Mol ID	Compounds	MW	AlogP	Hdon	Hacc	DL	Rotatable bonds	ADME
HQ1	*Scutellariae Radix*	Labiatae	MOL001689	Acacetin	284.28	2.59	2	5	0.24	2	yes
HQ2	*Scutellariae Radix*	Labiatae	MOL000173	Wogonin	284.28	2.59	2	5	0.23	2	yes
HQ3	*Scutellariae Radix*	Labiatae	MOL000228	(2R)-7-Hydroxy-5-methoxy-2-phenylchroman-4-one	270.3	2.82	1	4	0.2	2	yes
HQ4	*Scutellariae Radix*	Labiatae	MOL002560	Chrysin	254.25	2.6	2	4	0.18	1	yes
HQ5	*Scutellariae Radix*	Labiatae	MOL002714	Baicalein	270.25	2.33	3	5	0.21	1	yes
HQ6	*Scutellariae Radix*	Labiatae	MOL002737	Scutellarein	286.25	2.07	4	6	0.24	1	yes
HQ7	*Scutellariae Radix*	Labiatae	MOL002908	5,8,2′-Trihydroxy-7-methoxyflavone	300.28	2.32	3	6	0.27	2	yes
HQ8	*Scutellariae Radix*	Labiatae	MOL002909	5,7,2,5-Tetrahydroxy-8,6-dimethoxyflavone	376.34	2.02	4	9	0.45	4	yes
HQ9	*Scutellariae Radix*	Labiatae	MOL002910	Carthamidin	288.27	2.03	4	6	0.24	–	–
HQ10	*Scutellariae Radix*	Labiatae	MOL002913	Dihydrobaicalin_qt	272.27	2.3	3	5	0.21	1	yes
HQ11	*Scutellariae Radix*	Labiatae	MOL002914	Eriodyctiol (flavanone)	288.27	2.03	4	6	0.24	1	yes
HQ12	*Scutellariae Radix*	Labiatae	MOL002915	Salvigenin	328.34	2.82	1	6	0.33	4	yes
HQ13	*Scutellariae Radix*	Labiatae	MOL002917	5,2′,6′-Trihydroxy-7,8-dimethoxyflavone	330.31	2.3	3	7	0.33	3	yes
HQ14	*Scutellariae Radix*	Labiatae	MOL002918	Ganhuangenin	346.31	2.03	4	8	0.37	3	yes
HQ15	*Scutellariae Radix*	Labiatae	MOL002919	Viscidulin III	346.31	1.74	4	8	0.37	3	yes
HQ16	*Scutellariae Radix*	Labiatae	MOL002925	5,7,2′,6′-Tetrahydroxyflavone	286.25	2.07	4	6	0.24	1	yes
HQ17	*Scutellariae Radix*	Labiatae	MOL002927	Skullcapflavone II	374.37	2.54	2	8	0.44	5	yes
HQ18	*Scutellariae Radix*	Labiatae	MOL002928	Oroxylin a	284.28	2.59	2	5	0.23	2	yes
HQ19	*Scutellariae Radix*	Labiatae	MOL002932	Panicolin	314.31	2.57	2	6	0.29	3	yes
HQ20	*Scutellariae Radix*	Labiatae	MOL002933	5,7,4′-Trihydroxy-8-methoxyflavone	300.28	2.32	3	6	0.27	2	yes
HQ21	*Scutellariae Radix*	Labiatae	MOL002934	Neobaicalein	374.37	2.54	2	8	0.44	–	–
HQ22	*Scutellariae Radix*	Labiatae	MOL002936	5,8-Dihydroxy-6,7-dimethoxyflavone	314.31	2.57	2	6	0.29	3	yes
HQ23	*Scutellariae Radix*	Labiatae	MOL002937	Dihydrooroxylin	286.3	2.55	2	5	0.23	2	yes
HQ24	*Scutellariae Radix*	Labiatae	MOL000396	(+)-Syringaresinol	418.48	2.1	2	8	0.72	6	yes
HQ25	*Scutellariae Radix*	Labiatae	MOL000525	Norwogonin	270.25	2.33	3	5	0.21	1	yes
HQ26	*Scutellariae Radix*	Labiatae	MOL000552	5,2′-Dihydroxy-6,7,8-trimethoxyflavone	344.34	2.55	2	7	0.35	4	yes
HQ27	*Scutellariae Radix*	Labiatae	MOL000008	Apigenin	270.25	2.33	3	5	0.21	1	yes
HQ28	*Scutellariae Radix*	Labiatae	MOL008206	Moslosooflavone	298.31	2.84	1	5	0.25	3	yes
HQ29	*Scutellariae Radix*	Labiatae	MOL012240	2′,3′,5,7-Tetrahydroxyflavone	286.25	2.07	4	6	0.24	1	yes
HQ30	*Scutellariae Radix*	Labiatae	MOL012245	5,7,4′-Trihydroxy-6-methoxyflavanone	302.3	2.28	3	6	0.27	2	yes
HQ31	*Scutellariae Radix*	Labiatae	MOL012246	5,7,4′-Trihydroxy-8-methoxyflavanone	302.3	2.28	3	6	0.26	–	–
HQ32	*Scutellariae Radix*	Labiatae	MOL012266	Rivularin	344.34	2.55	2	7	0.37	4	yes
HQ33	*Scutellariae Radix*	Labiatae	MOL012267	Scutevulin	300.28	2.32	3	6	0.27	2	yes
DH1	*Radix Rhei* et *Rhizome*	Polygonaceae	MOL001729	Crysophanol	254.25	2.76	2	4	0.21	0	yes
DH2	*Radix Rhei* et *Rhizome*	Polygonaceae	MOL002235	Eupatine	360.34	1.99	3	8	0.41	4	yes
DH3	*Radix Rhei* et *Rhizome*	Polygonaceae	MOL002258	Physcion-9-*O*-beta-*D*-glucopyranoside_qt	300.28	2.48	3	6	0.3	–	–
DH4	*Radix Rhei* et *Rhizome*	Polygonaceae	MOL002268	Rhein	284.23	1.88	3	6	0.28	1	yes
DH5	*Radix Rhei* et *Rhizome*	Polygonaceae	MOL002281	Toralactone	272.27	2.25	2	5	0.24	1	yes
DH6	*Radix Rhei* et *Rhizome*	Polygonaceae	MOL002286	Laccaic acid D	300.23	1.61	4	7	0.31	–	–
DH7	*Radix Rhei* et *Rhizome*	Polygonaceae	MOL000471	Aloe-emodin	270.25	1.67	3	5	0.24	1	yes
DH8	*Radix Rhei* et *Rhizome*	Polygonaceae	MOL000472	Emodin	270.25	2.49	3	5	0.24	0	yes
DH9	*Radix Rhei* et *Rhizome*	Polygonaceae	MOL000476	Physcion	284.28	2.74	2	5	0.27	1	yes

Notes: Mol ID, ID information of drug as defined in TCMSP; MW, molecular weight; Alog*P*, value of partition coefficient measured by ACD; Hdon, number of H-bond donor; Hacc, number of H-bond acceptor; DL, drug-likeness; ADME, absorption, distribution, metabolism, and excretion. "–" indicats that these compounds do not have a Pubchem Cid and cannot obtain a Smile or SDF format file.

(Table S2). A total of 442 nodes and 2 999 edges were predicted as the general characteristics of the network analysis (Fig. 1). According to the topological degree, we selected 16 compounds as the key ingredients (Table S3).

3.2. RSVP targets searching

As mentioned earlier, four disease target databases were used to integrate 1 047 genes related to RSVP. The following GEO series were selected, and data were downloaded from the platform: GSE6802 (Mayer et al., 2007), GSE77087 (de Steenhuijsen Piters et al., 2016), and GSE38900 (Mejias et al., 2013). Samples: GSM157034-GSM157036, GSM2043626-GSM2043729, GSM951640-GSM951666, GSM951668-GSM951669, GSM951672, GSM951674-GSM951781. A total of 57 normal samples and 191 RSVP samples were collected in total. We attained 738 genes with significant distinctions based on the filtration system. The volcano plot was shown in Fig. 2, with the red upregulated and green downregulated genes. After collecting all the genes and removing duplicate data, there were 1 626 remained for further research (Table S4). Finally, the Venn diagram displayed 131 genes as the implicit aim of the new preparation for the therapies of RSVP (Fig. 3A).

3.3. PPI analysis

We imported 131 potential targets into STRING, and finally, 110 potential targets through the screening threshold were obtained

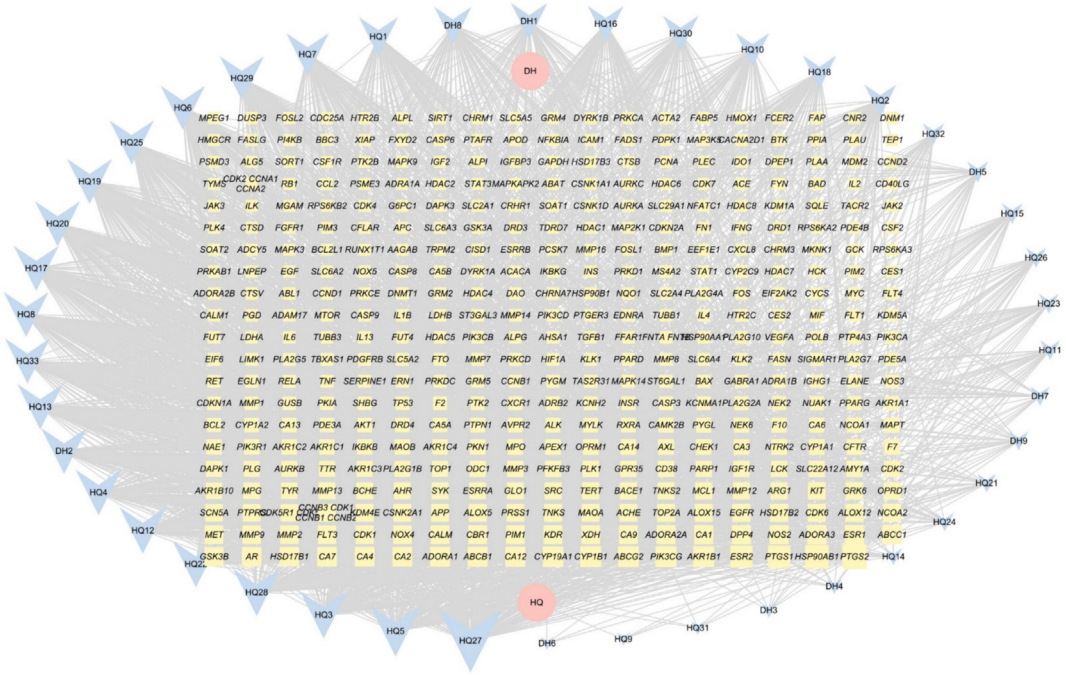

Fig. 1. "Drug-chemical composition-target" network. Pink ellipse represents medicinal herb of QFP; blue V-shape represents critical components screened out by QFP. Yellow rectangle represents key target points screened out, and edge connects target to active ingredient. The more significant number of links and the larger nodes indicate that active ingredient or target is more critical in network with higher degree value.

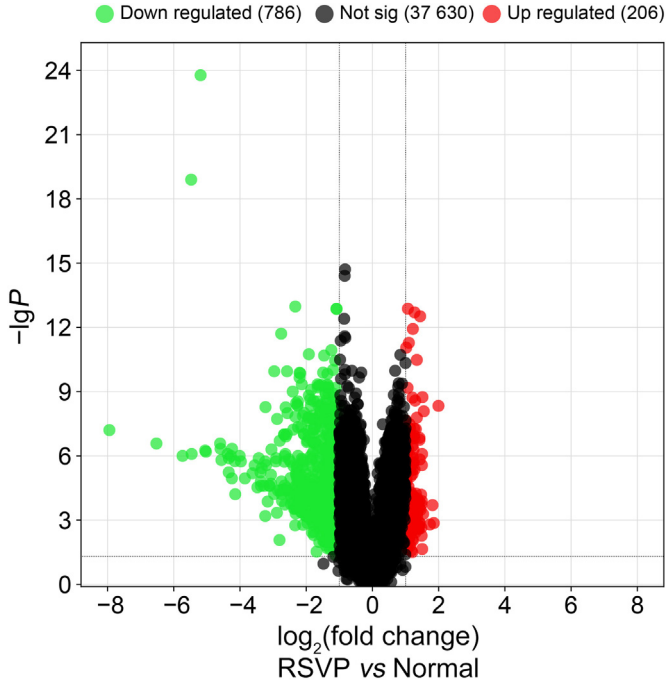

Fig. 2. RSVP differential gene volcano map.

(Fig. 3B). Then, we represented a PPI network (110 nodes and 506 edges) after importing target genes into Cytoscape 3.9.1 software (Fig. 3C). Increasing quantified values were related to the improved significance of the node. The topological analysis of key targets was based on the Degree, CC, BC > one-fold of the median. A total of 49 key gene targets were first sorted with the subsequent standards: Degree > 6, CC > 0.43, BC > 0.003, and 19 key gene targets (*TNF*, *NOS2*, *MAPK14*, *CCND1*, *STAT1*, *SRC*, *TP53*, *IL6*, *HIF1A*, *AKT1*, *STAT3*, *HSP90AA1*, *JAK2*, *CDKN1A*, *MAPK3*, *EGFR*, *MYC*, *FOS* and *RELA*) were second sorted with the subsequent standards: Degree > 12, CC > 0.476, BC > 0.012 (Table S5).

3.4. GO terms and KEGG pathways

Through GO and KEGG analysis of the 131 intersection targets, 2 120 GO terms were identified. Of these, 1 878 were biological process items, mainly protein phosphorylation, positive regulation of kinase activity, and regulation of protein kinase activity. Additionally, 146 molecular function items were shown to be mainly associated with protein kinase activity, kinase binding, and cytokine receptor binding. We also identified 96 cell component entries, mainly involving cytoplasmic vesicle lumen, receptor complex, extracellular matrix, and mitochondrial envelope. Furthermore, 190 KEGG enrichment entries were obtained, generally associated with pathways such as the P13K-AKT pathway, HIF-1 pathway, IL-17 signaling pathway, hepatitis B pathway, and pathways in cancer. According to the enrichment count, the top 20 GO terms and KEGG analysis were concentrated (Fig. 4A–D). Finally, we constructed a "drug-target-KEGG pathways" network (Fig. 4E) and provided detailed information in Table S6.

3.5. Molecular docking verification

The binding free energy of each target was shown in Fig. 5A (heatmap). Except for skullcapflavone II and EUPATIN, other core compounds had an excellent binding affinity to specific core targets (only the binding energies < −5 kcal/mol were demonstrated). Among them, the most substantial binding was between baicalein and EFGR (−7.2 kcal/mol); meanwhile, the weakest binding was between scutevulin and MAPK14 (−5.01 kcal/mol). The relatively large number of core targets bound by baicalein, chrysin, apigenin, and emodin suggested that they might be the most influential ingredients in the mechanism of QFP treatment of RSVP. The components in the highest binding energy of each target protein were

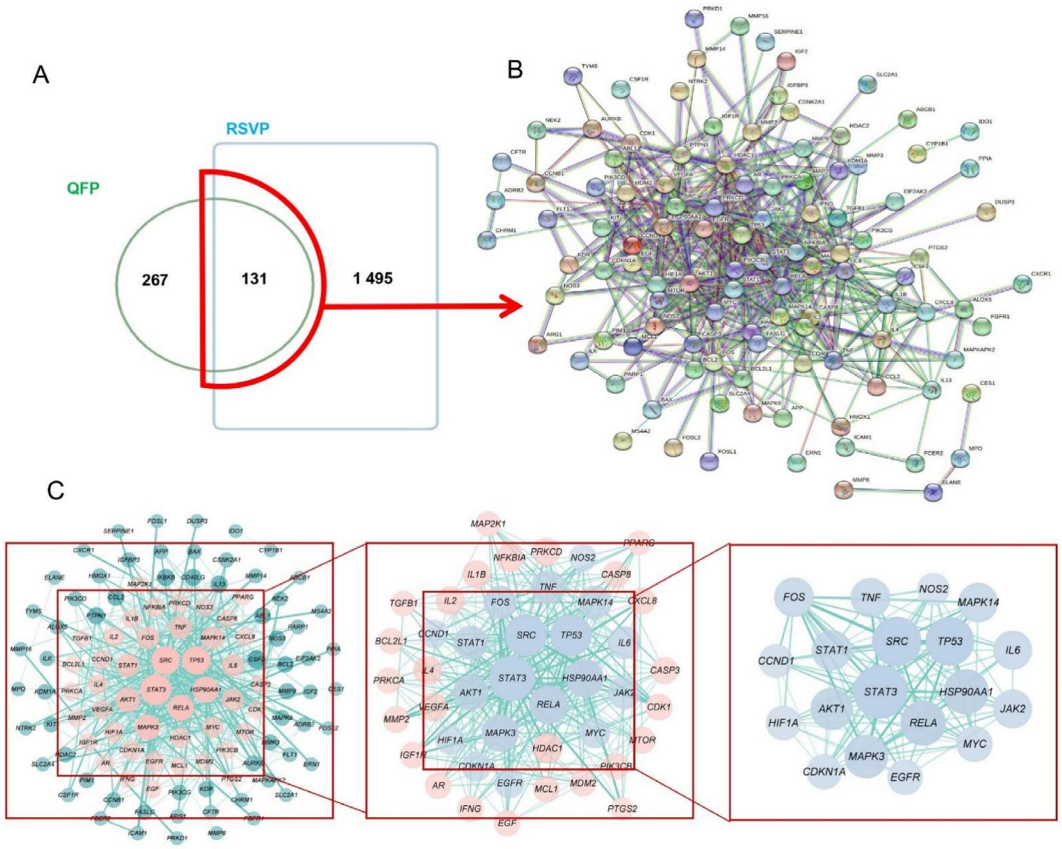

Fig. 3. Common targets of QFP and RSVP. (A) Venn plot. (B) PPI network diagram. (C) Screening topology of core targets.

visualized by PyMOL (Fig. 5B). EGFR was the protein receptor with the most significant number of bindings, suggesting that it played a prominent role in the mechanism of the RSVP. Contrary to the topology results, molecular docking showed that IL6 and STAT1 did not bind directly spatially to any vital chemical synthetic components, indicating that IL6 and STAT1 may be downstream of some cascade reactions. The results indicated that except for skullcapflavone II and EUPATIN, the key ingredients of QFP in the treatment of RSVP had an estimable binding ability with each key protein target.

3.6. QFP improved lung pathological conditions of RSVP rats

To quantify pulmonary inflammation, we explored the effect of QFP treatment on the pulmonary pathology of RSVP rats. Firstly, the gross pulmonary lesions were recorded *in vivo*. The lungs of the model rats were significantly hyperemic and edematous. Comparatively, the edema and the regions of hemorrhage decreased after the treatment of QFP (Fig. 6A). Secondly, HE-stained pathological sections of lung tissue were observed under light microscopy. No significant pathological changes in the normal group existed, with the normal structure of bronchi, alveoli, and alveolar septa and almost no alveoli infiltrated by inflammatory cells. However, the model rats displayed significant thickening of the walls of bronchioles and vessels, accompanied by edema of surrounding tissues. Abundant inflammatory cells aggregated in the walls of alveoli, bronchioles, and vessels and the alveolar wall was significantly thickened. Some of the alveoli had significant collapse or expansion, forming emphysema changes. The QFP group was identified with improved pathological changes, which showed decreased edema of surrounding tissues, inflammatory cell infiltration, and alveolar wall thickness (Fig. 6B). Distinguished from the Mod group, the pathological score of the QFP group was considerably reduced (Fig. 6C). In summary, pulmonary pathology was substantially improved after QFP treatment.

To further identify the pathology of the lungs, we also explored the lung index. This marker can indirectly indicate the severity of pulmonary edema (Perchiazzi et al., 2022) as a complement to histopathology sections. Opposed to the Nor group, the lung index of the Mod group rose and then decreased significantly after QFP treatment (Fig. 6D).

3.7. QFP reduced amount of IL-6 in blood

Next, we demonstrated some of the results in the network pharmacological prediction. In RSVP, the content of some serum cytokines can reflect immunomodulation of inflammation and accumulation of inflammatory cells. IL-6, an inflammatory mediator that macrophages and epithelial cells can produce (Jones & Jenkins, 2018), has been emphasized as a prognostic molecule in human RSV (hRSV) infections due to its essential involvement in the anti-hRSV immunity in the host as a pro-inflammatory cytokine (McNamara, Flanagan, Selby, Hart, & Smyth, 2004). Therefore, we examined whether QFP could downregulate IL-6 expression. ELISA results demonstrated that QFP could partially suppress systemic inflammation with decreased IL-6 (Fig. 6E).

3.8. QFP effectively inhibited PI3K/AKT pathway, HIF-1A and NOS2 after RSV infection

Finally, we verified the expression of the PI3K/AKT signaling pathway in the lungs of RSVP rats. As shown in Fig. 7, there were no significant changes in PI3K and AKT proteins after RSV infection and QFP intervention. The model group showed significantly

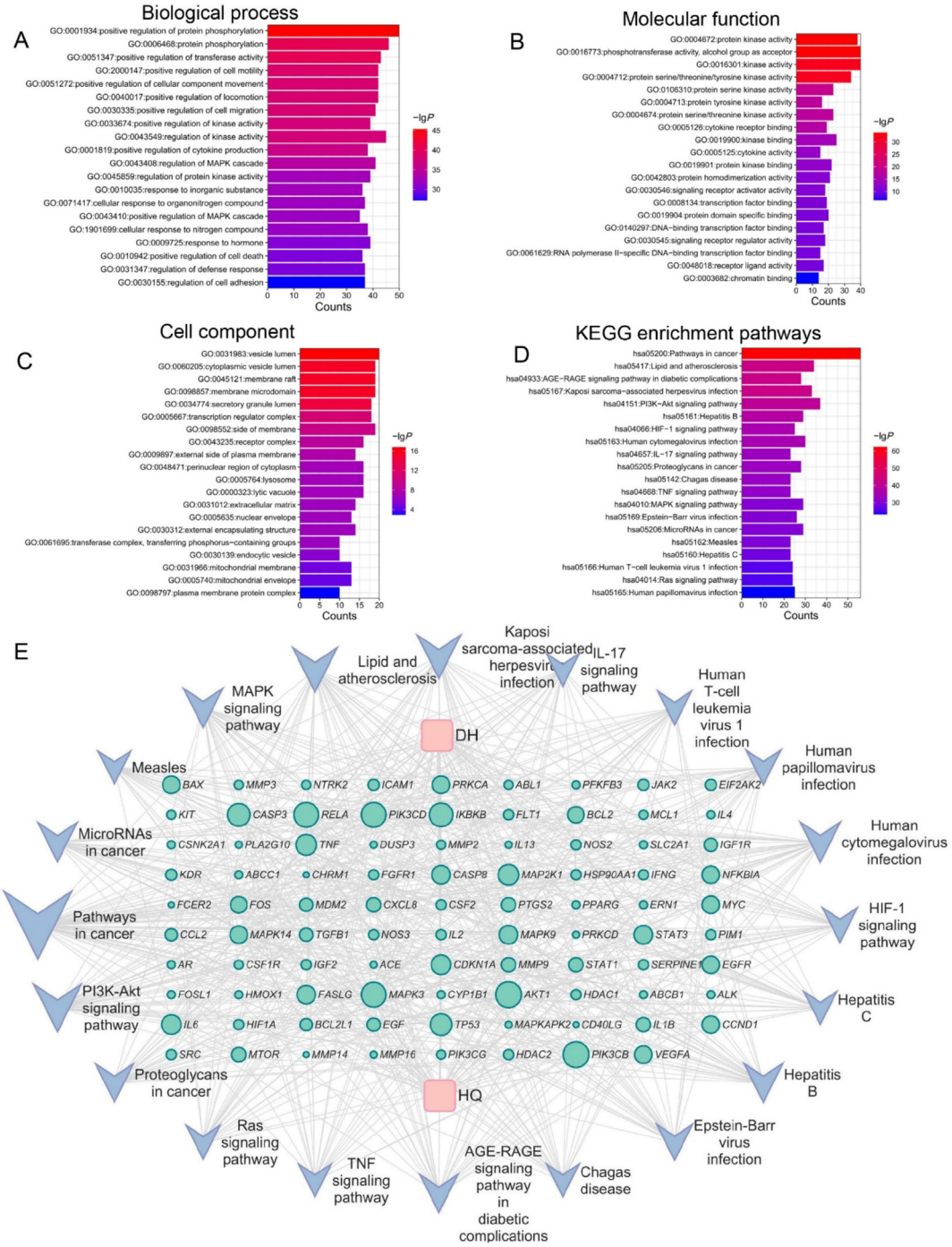

Fig. 4. GO and KEGG analysis of QFP for treatment of RSVP. (A) Biological process. (B) Molecular function. (C) Cell component. (D) KEGG enrichment pathways. (E) "Drug-target-KEGG pathways" network. Genes are shown as green circles, pathways are represented as blue V-shapes, and drugs are shown as pink round rectangles.

increased levels of p-PI3K and p-AKT, while QFP treatment reduced levels of p-AKT. However, there was no significant change in the level of p-PI3K between the model and the QFP groups. The expression of HIF-1A and NOS2 was enhanced in the model group and decreased after QFP intervention.

3.9. QFP improved serum metabolic disorders induced by RSVP based on multivariate statistical analyses

To further explore the changes in serum metabolites in RSVP rats after QFP administration, the OPLS-DA model in multivariate statistical analysis was used to predict each set of sample classes. The significant separation of three groups from the ESI^+ and ESI^- modes perceived differential samples among the normal, model, and QFP groups (Fig. 8A–H). The permutation test showed that none of the Q^2 regression line intercepts were larger than 0, demonstrating that the OPLS-DA model was not overfitted. These data showed that QFP could correct metabolic disorders in RSVP rats.

3.10. Potential biomarkers screening

A total of 292 candidate metabolites were detected in three groups (Table S7), and metabolites with a VIP-value > 1.0 were

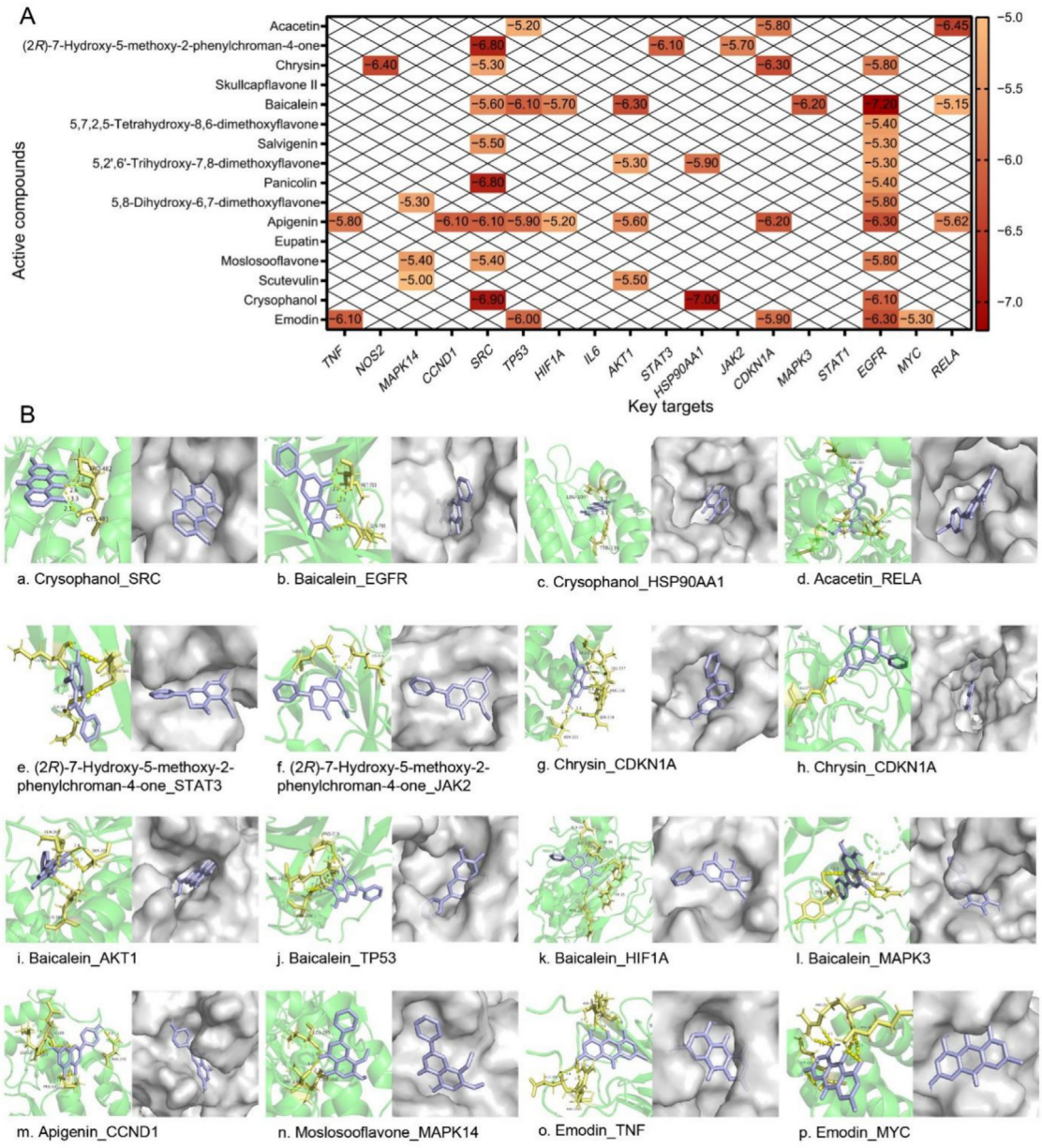

Fig. 5. (A) Thermographic analysis of molecular docking binding energies. (B) Visualization of the highest binding energy between 16 core targets and active compounds (a–p). Blue sticks indicate chemical composition, and yellow sticks indicate binding sites on target protein. The surface of target proteins is selected as grey to show pocket structure.

considered potential biomarkers. Eventually, a total of 28 metabolites were considered potential biomarkers. As shown in the box plot, blue represents the normal group, red represents the model group, and green represents the QFP group (Fig. 9). To comprehensively visualize the difference in the expression pattern of metabolites among the samples, a hierarchical cluster analysis of each group sample was performed based on the expression amounts of differential metabolites (Fig. 10). This heatmap showed an increase in biomarker abundance from blue to red colors. A total of 18 biomarkers were increased, and 10 biomarkers decreased markedly after RSV infection.

3.11. Metabolic pathway analysis of RSVP with QFP treatment

The analysis was presented with MetaboAnalyst 5.0 to visualize the metabolic processes of QFP treatment in RSVP rats. We selected eight significant potential pathways with an impact value above 0.10 (Fig. 11, Table 2), which were generally associated with lipid and amino acid metabolism. The results indicated that linoleic acid metabolism was carried into effect in the QFP treatment on RSVP.

After the screening, a total of 13 pathways [bile secretion, chemical carcinogenesis-receptor activation, ABC transporters, Gap junction, central carbon metabolism in cancer, diabetic cardiomyopathy, insulin resistance, intestinal immune network for IgA production, arginine biosynthesis, small cell lung cancer, cyclic adenosine monophosphate (cAMP) signaling pathway, Th17 cell differentiation, and gastric cancer] are common to the metabolic pathway and the KEGG pathway. The important biomarkers, targets, and pathways were eventually validated by comparing the prospective hub targets and pathways found in network pharmacology to the potential biomarkers and metabolisms found in the metabolomic analysis. We have established a "pathway-metabolite-target-compound" network. As shown in Fig. 12, in addition to the 13 pathways, 21 differential metabolites had been identified

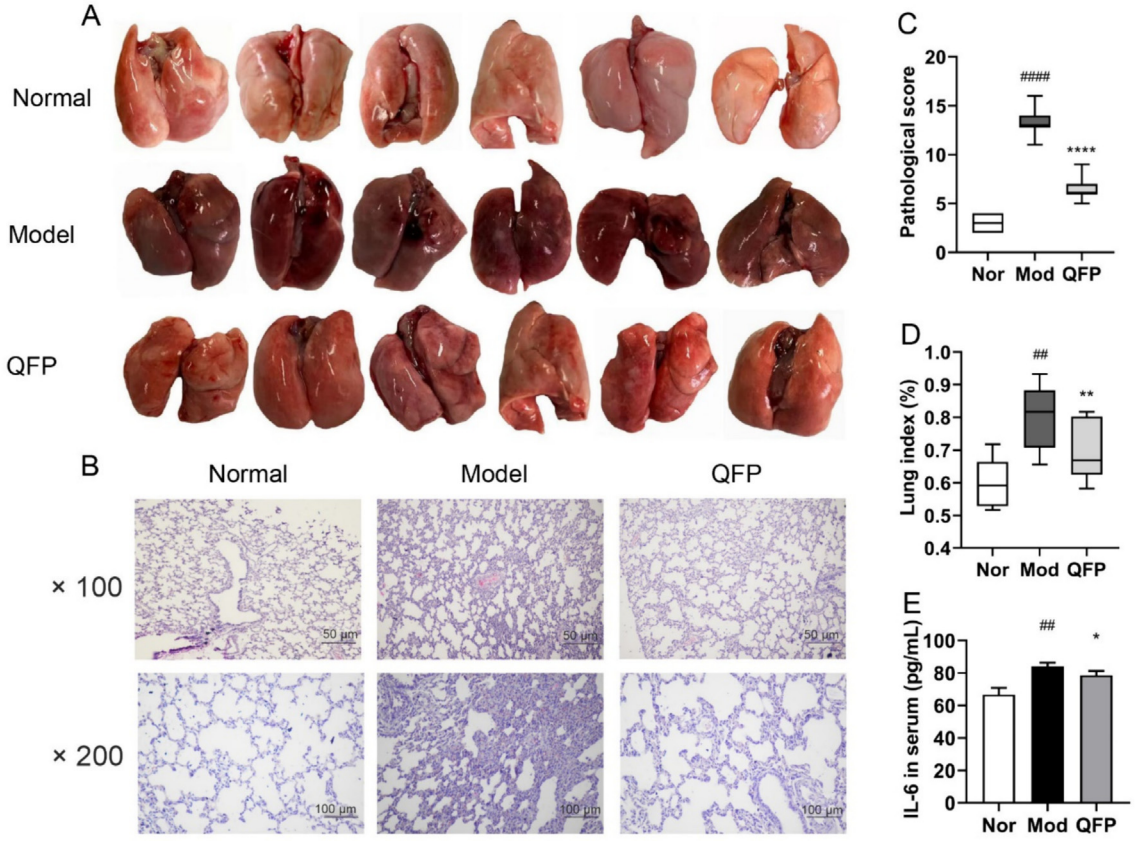

Fig. 6. Effect of QFP on lung lesions in RSVP rats (mean ± SD; $n = 6$). (A) Gross macroscopic structure of lungs. (B) Pathological examination of lungs after HE staining (scale bar = 50 μm, × 100 and scale bar = 100 μm, × 200). (C) Pathological score of rats. $^{\#\#\#\#}P < 0.000\ 1$ *vs* normal group, $^{****}P < 0.000\ 1$ *vs* model group. (D) Lung index of rats. $^{\#\#}P < 0.01$ *vs* normal group, $^{**}P < 0.01$ *vs* model group. (E) Effects on IL-6. $^{\#\#\#}P < 0.001$ *vs* normal group, $^{*}P < 0.05$ *vs* model group.

[of which glutamic acid, TXB2, retinoic acid, *L*-carnitine, serotonin, and glutathione (oxidized) were significant differential metabolites], 19 core targets (*TNF*, *NOS2*, *MAPK14*, *CCND1*, *STAT1*, *SRC*, *TP53*, *IL6*, *HIF1A*, *AKT1*, *STAT3*, *HSP90AA1*, *JAK2*, *CDKN1A*, *MAPK3*, *EGFR*, *MYC*, *FOS,* and *RELA*) were also thought to play a crucial role in the therapeutic effect of QFP on RSVP.

4. Discussion

The complex host immunoreaction to RSV infection is connected to multiple molecular components, manifested by the coexistence of inflammation caused by viruses and their antiviral properties (Tahamtan et al., 2021). Subsequently, the body reaction exacerbates significant pathogen-associated pulmonary inflammation by promoting viral clearance in most cases (Openshaw, Chiu, Culley, & Johansson, 2017). Studies reported the generally weak inductions of humoral responses and virus-specific antibodies by RSV infections, which might partially cause insufficient adaptive memory immunity response to natural infections (Blunck et al., 2021; Habibi et al., 2015; Van Royen, Rossey, Sedeyn, Schepens, & Saelens, 2022). The developing morphology with narrower bronchioles of infant airways increases the severity and morbidity of bronchiolitis or pneumonia (Damasio et al., 2015; Nair et al., 2010), and RSV possibly generates symptomatic reinfection in subsequent life (Openshaw, Chiu, Culley, & Johansson, 2017). One South African cohort of children under 5 years old reported RSV was most strongly related to recurrent wheezing of all viruses detected, leading to high airway resistance (McCready et al., 2023). Therefore, the efficient intervention of RSVP is necessary for children.

QFP is administered transdermally in the treatment of RSVP. Based on the formulation considerations for passive transdermal delivery and ideal limits, our research included the oil–water partition coefficient (Log*P*), molecule weight, and Lipinski rules of five as crucial parameters in predicting absorption into the blood. We sorted the compounds and targets of QFP from multiple databases and set up a "compound-gene target-disease" network. CytoNCA software was used to estimate key protein targets based on topological analysis and obtain the essential targets involved in RSV inflammations, including AKT1, EGFR, IL6, TNF, HIF1A, RELA, MAPK14, MAPK3, STAT1, and STAT3. We identified multiple inflammatory response-related signaling pathways in KEGG pathway analysis, suggesting that inflammation was the most prominent penetration point in curing RSVP. Subsequently, to elucidate the pathogenesis of RSVP and establish a prospective network model, we ignored a list of irrelevant pathways in the top 20 most enriched pathways, like lipid and atherosclerosis and human papillomavirus infection. We found that the top five pathways associated with the inflammatory response enriched by network pharmacology were the PI3K/AKT pathway, MAPK pathway, IL-17 pathway, HIF-1 pathway, and TNF pathway. We identified the PI3K/AKT pathway and HIF-1 pathway through literature review and enrichment counting as key inflammation-related processes in the treatment of RSVP by QFP, so we validated several key markers *in vivo*, such as PI3K, p-PI3K, AKT, p-AKT, and HIF-1A. A screening for serum metabolomics was finally performed, allowing us to explain further the mechanism of QFP treatment for RSVP with dif-

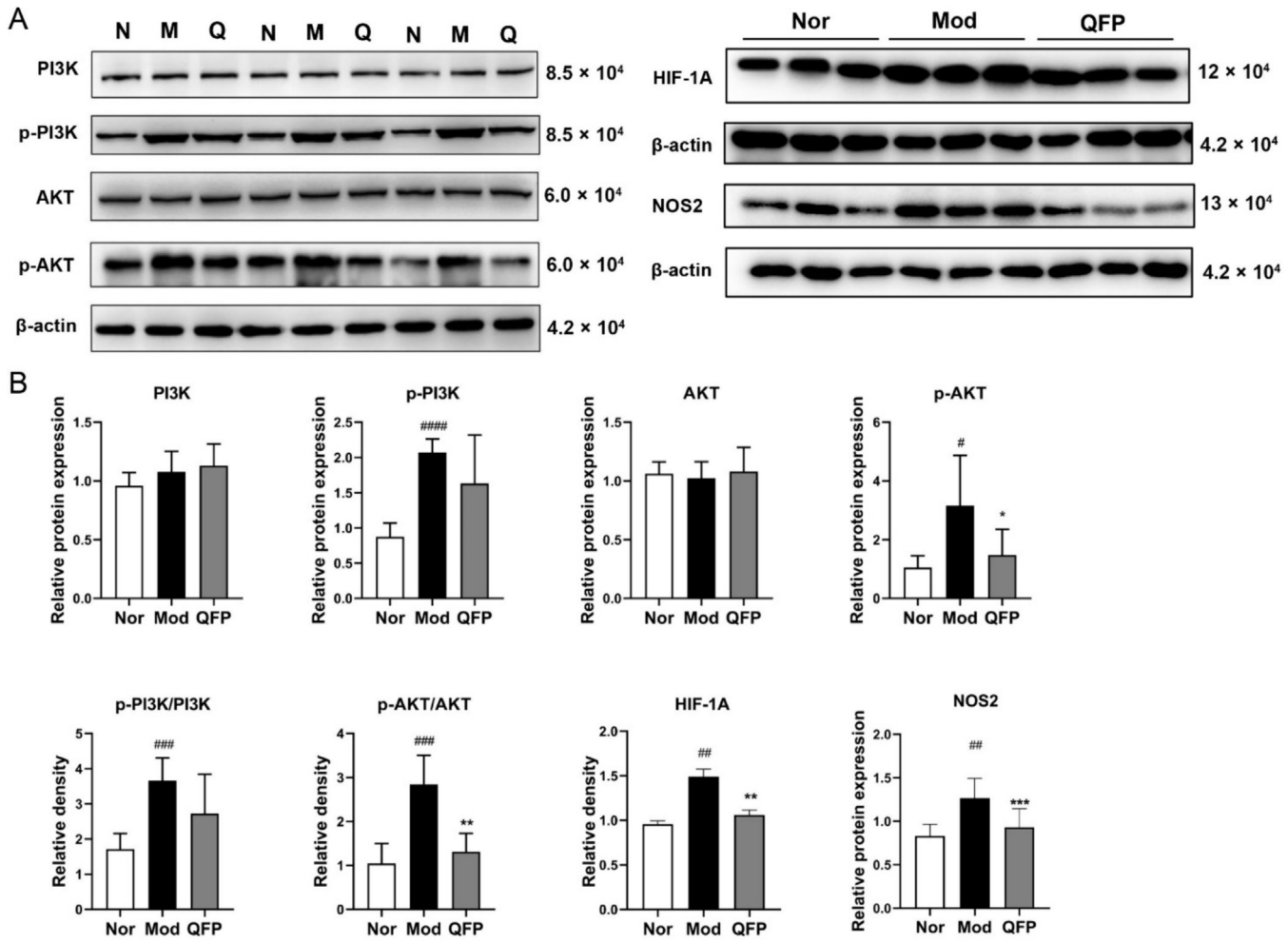

Fig. 7. QFP partially suppressed phosphorylation of PI3K and AKT in RSVP rats and inhibited expression of HIF-1α and NOS2 proteins (mean ± SD; $n = 6$). (A) Representative blots in lungs. (B) Western-blot analysis of protein expressions of PI3K, AKT, p-PI3K, p-AKT, HIF-1α, NOS2, and β-actin served as an internal control. $^{\#}P < 0.05$, $^{\#\#}P < 0.01$, $^{\#\#\#}P < 0.001$, $^{\#\#\#\#}P < 0.000\ 1$ *vs* normal group; $^{*}P < 0.05$, $^{**}P < 0.01$, $^{***}P < 0.001$ *vs* model group. Note: N, M, and Q correspond to samples from normal, model, and QFP groups, respectively.

ferential metabolites and metabolic pathways. And the QFP intervention reversed some key metabolites' levels and influenced significant metabolic pathways.

The expression of PI3K/AKT proteins in rat lungs was measured by western blot. The bands showed significant PI3K/AKT phosphorylation after RSV infection, but the effect of QFP on p-AKT was more pronounced compared with p-PI3K. PI3K phosphorylation acts as a secondary messenger that modulates the phosphorylation of the serine/threonine kinase AKT (Manning & Cantley, 2007). AKT's phosphorylation acts as a reliable indicator of the activation of PI3K signaling, as it is a major downstream effector of PI3K signaling (Mannová & Beretta, 2005). The PI3K/AKT pathway facilitates replication via RSV by inhibiting or delaying apoptosis in airway epithelial cells. Through direct phosphorylation, activated AKT inhibits downstream apoptotic promoters, such as Bad and caspases (Bitko et al., 2007; Groskreutz et al., 2007; Thomas et al., 2002). A study in RSV-infected human lung fibroblasts found that AKT was directly phosphorylated (Seki et al., 2013). Our research demonstrated that the primary role site of QFP in the PI3K/AKT pathway was AKT, which coincided with the prediction of the core target by CytoNCA. However, the role of PI3K-AKT in lung injury was controversial. Some studies have shown that activation of the PI3K-AKT pathway can alleviate lung inflammation (Li et al., 2022; Pu, Shen, Zhang, Xie, & Wang, 2022). These results may be inconsistencies due to differences in pathogens causing inflammation, animal models, and specimen collection time points. We will collect specimens from multiple time points in the same RSV pneumonia animal model to validate our conclusions. HIF-1 has been demonstrated to have a transcriptional coordinating function in inflammatory and infectious processes, making it one of the most effective biological triggers for creating an inflammatory environment (Taylor & Colgan, 2017). Recent *in vivo* studies suggest RSV can cause HIF-1α stability and accumulation through non-hypoxic routes (Morris, Qu, Agrawal, Garofalo, & Casola, 2020), as demonstrated in our rat model. We speculated that HIF-1α, as a downstream factor of PI3K/AKT, mediated immune response and inflammation. Our study demonstrated the inhibition of HIF-1α by QFP, suggesting that QFP might relieve lung inflammation by inhibiting PI3K/AKT/HIF-1α. NOS2 can induce the production of nitric oxide (NO) as an early immune mediator to address pathogen challenges. Pro-inflammatory cytokines generated by inflammatory cells can potentially increase *NOS II* gene transcription in response to direct cellular infection or a paracrine manner (Tsutsumi, Takeuchi, Ohsaki, Seki, & Chiba, 1999). We also observed RSV-induced NOS2 elevation in rat models, consistent with other studies. Decreased NOS2 after QFP intervention may indicate the anti-inflammatory effects of QFP, but high expression of NOS2 has also been suggested to accelerate RSV clearance

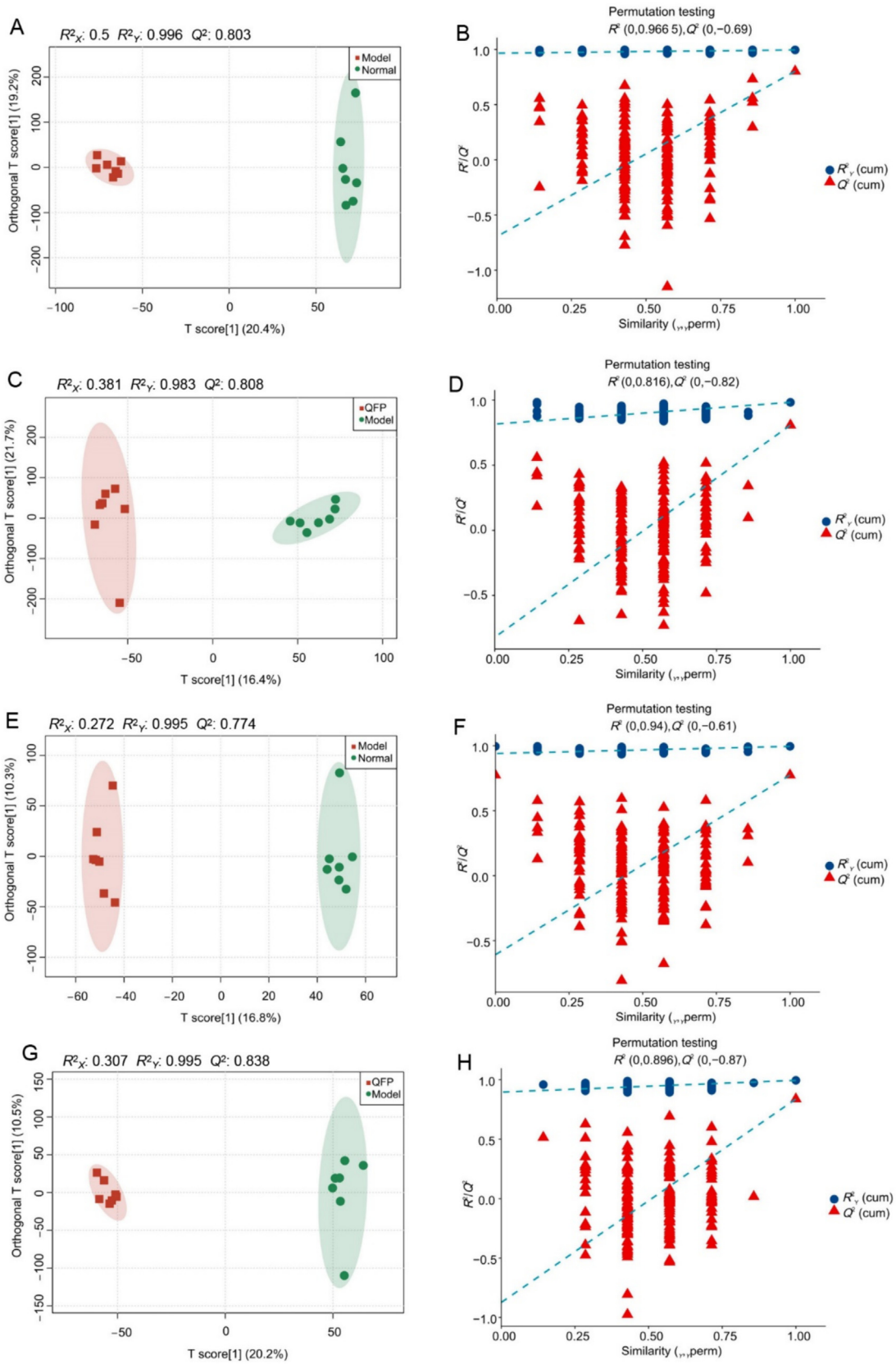

Fig. 8. OPLS-DA score plots and 100-permutation test were generated from OPLS-DA data of normal, model, and QFP groups. (A, E) OPLS-DA score scatter plots for pairwise comparisons between model and normal groups. (C, G) OPLS-DA score scatter plots for pairwise comparisons between QFP and model groups. (B, F) 100-permutation test of OPLS-DA model between model and normal groups. (D, H) 100-permutation test of OPLS-DA model between QFP and model groups. Notes: (A–D) ESI^+ model; (E–H) ESI^- model.

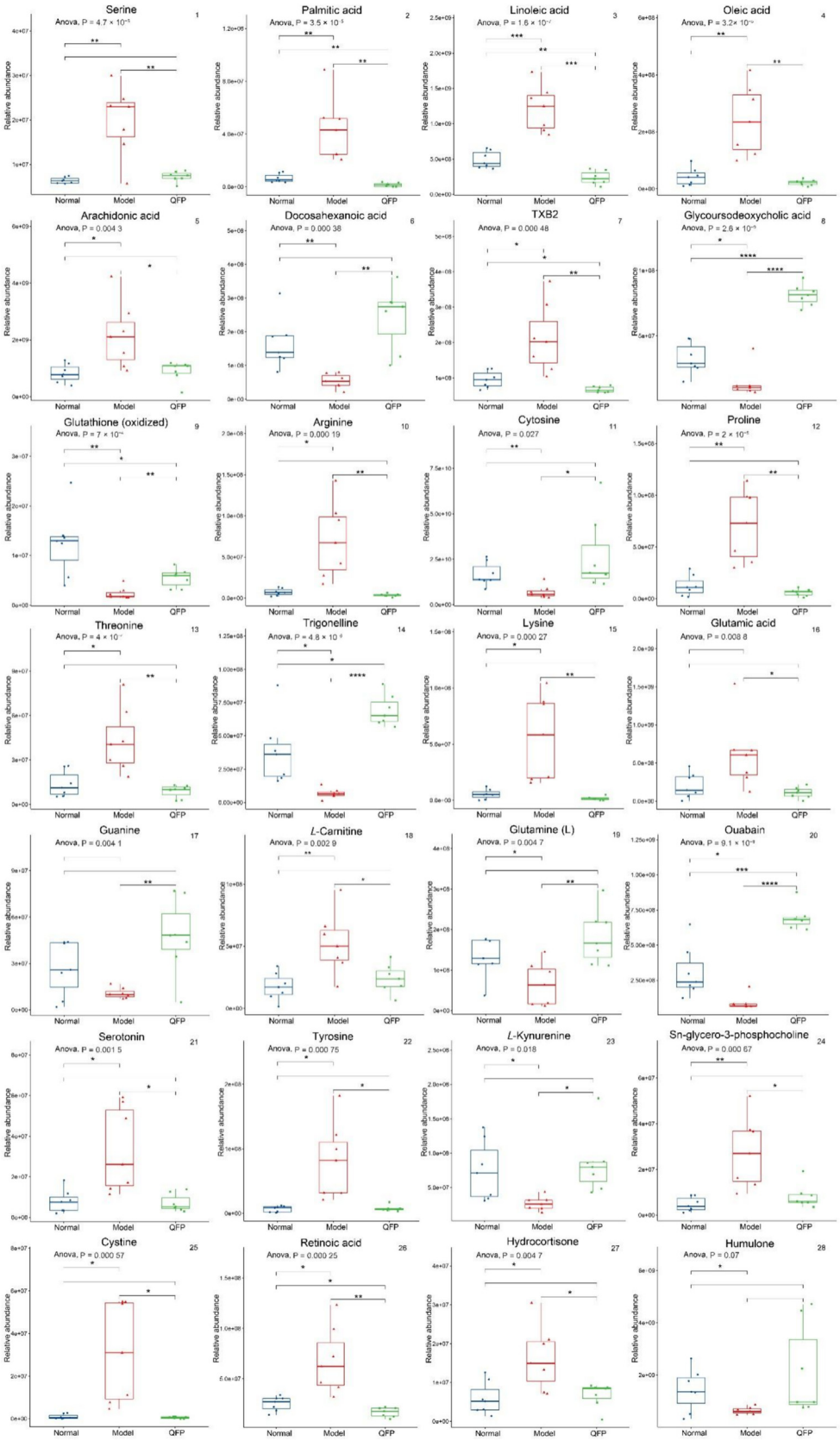

Fig. 9. Potential differential metabolites changes in RSVP with QFP treatment. 1–28 represent 28 metabolites. Results are expressed as mean ± SD (n = 7). $^{*}P < 0.05$, $^{**}P < 0.01$, $^{***}P < 0.001$, $^{****}P < 0.000\ 1$.

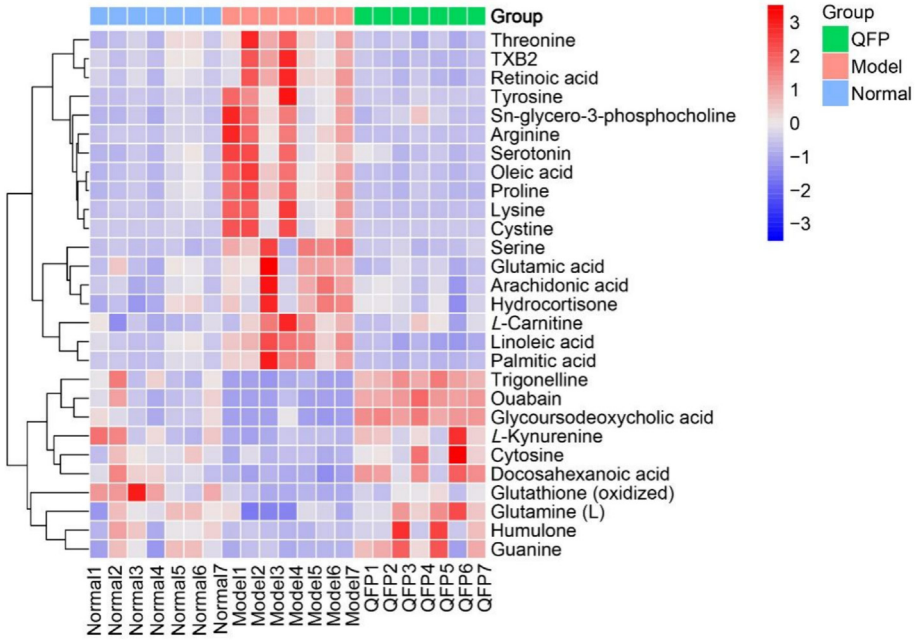

Fig. 10. Cluster heatmap of potential metabolites in each group.

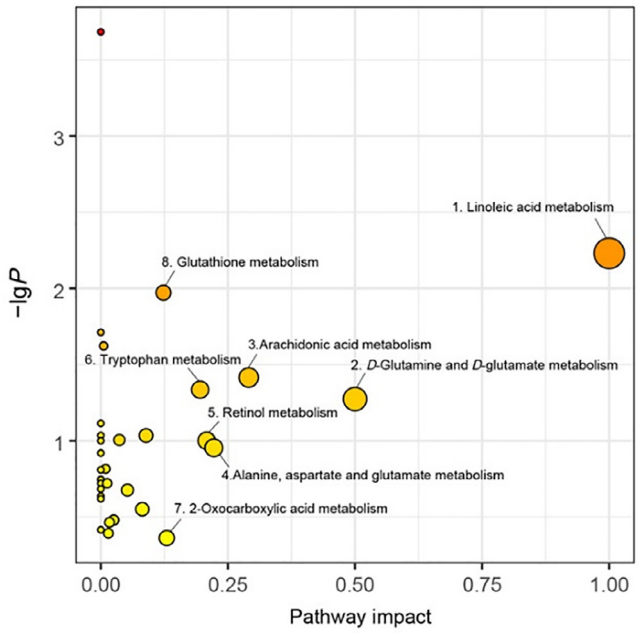

Fig. 11. Main metabolomic pathways involved in effects of QFP on RSVP. Size of bubbles represents influence of pathway.

(Phipps et al., 2007). The role of NOS2 during the persistence of RSV viruses requires further study. A single-center analysis showed an inflammatory phenotype in 16 with severe RSV bronchiolitis through paired transcriptomic analysis, characterized by upregulated expression of IL-6 pathways (Besteman et al., 2020). Our Elisa results demonstrated that QFP had an excellent down-regulation effect on IL-6.

We simulated the molecular docking of candidate chemical ingredients to targets. Our results revealed that the most potent compound was apigenin, which bound most proteins. Apigenin, a flavonoid, has demonstrated anti-RSV activity in human larynx epidermoid carcinoma cell lines (Wang et al., 2012) and has direct involvement in regulating inflammation and apoptosis (Vargas et al., 2015). In addition, baicalein and emodin also joined many protein receptors. Baicalein is an active ingredient isolated from *Scutellariae Radix* that can depress pro-inflammatory factor expression and T lymphocyte infiltration and partially reverse lung damage and inflammation caused by RSV infection, exhibiting potent anti-inflammatory and antiviral effects (Shi et al., 2016). Another research reported the ability of baicalein to anti-virus by increasing the TNF-α and other cytokines levels in RSV rats' serum (Cheng, Wu, Gao, & Xu, 2014). Emodin has been certified to expose plentiful bioactivities such as antiviral, anti-inflammatory, and antimicrobial. Experiments *in vitro* have demonstrated that emodin can indirectly fight the virus in a concentration- and time-dependent manner within 0−4 h after infection with RSV (Liu, Ma, Zhong, & Yang, 2015). On the other hand, the most popular protein receptor was EGFR, which could dock with 11 ligands. EGFR is a tyrosine kinase receptor that can be activated after RSV infection to induce airway epithelial inflammation, and F protein-mediated EGFR phosphorylation contributes to mucin production (Currier et al., 2016). It has been reported that inhibition of EGFR can reduce RSV titers by upregulating interferon-gamma (IFN-γ) (Kalinowski et al., 2018). Secondly, SRC, a tyrosine-protein kinase, has been shown to combine eight ligands. RSV invasion depends on the activation of c-SRC, and it is noteworthy that SRC can regulate the activation and phosphorylation of EGFR as an upstream factor (Lingemann et al., 2019). The co-activation leads to efficient uptake of RSV, which corresponds to our results. Surprisingly, two compounds and two proteins without effective docking (binding energy higher than −5.0 kcal/mol). Nonetheless, based on numerous confirmed consequences, we still recognize their importance in treating RSVP rather than neglecting their participation simply because of the molecular docking analysis. Finally, our results demonstrate that TCM has a multi-target effect, confirming the affinity between QFP and a series of physiological changes.

We detected endogenous biomarkers to further explain the efficacy of QFP from an overall functional status. We explored the disordered metabolic processes before and after QFP treatment by applying metabolomics in serum. The results suggested that RSVP

Table 2
Metabolic pathway analysis.

No.	ID	Descriptions	Metabo ratio	*P* value	*P* adjust	*q* value	Second Class	Top Class	Impact BC
1	rno00591	Linoleic acid metabolism	2/18	0.005 882 23	0.054 704 735	0.027 863 193	Lipid metabolism	Metabolism	1
2	rno00471	*D*-Glutamine and *D*-glutamate metabolism	1/18	0.053 217 417	0.097 043 524	0.049 427 941	Metabolism of other amino acids	Metabolism	0.5
3	rno00590	Arachidonic acid metabolism	2/18	0.038 449 044	0.091 686 182	0.046 699 244	Lipid metabolism	Metabolism	0.290 9
4	rno00250	Alanine, aspartate and glutamate metabolism	1/18	0.111 296 78	0.148 601 835	0.075 688 541	Amino acid metabolism	Metabolism	0.222 3
5	rno00830	Retinol metabolism	1/18	0.099 957 129	0.136 706 074	0.069 629 579	Metabolism of cofactors and vitamins	Metabolism	0.208 2
6	rno00380	Tryptophan metabolism	2/18	0.046 231 574	0.093 468 182	0.047 606 884	Amino acid metabolism	Metabolism	0.195 3
7	rno01210	2-Oxocarboxylic acid metabolism	1/18	0.435 500 717	0.435 500 717	0.221 817 003	Global and overview maps	Metabolism	0.129 7
8	rno00480	Glutathione metabolism	2/18	0.010 671 997	0.065 222 349	0.033 220 212	Metabolism of other amino acids	Metabolism	0.123 2

Note: Impact BC, impact value of potential pathway.

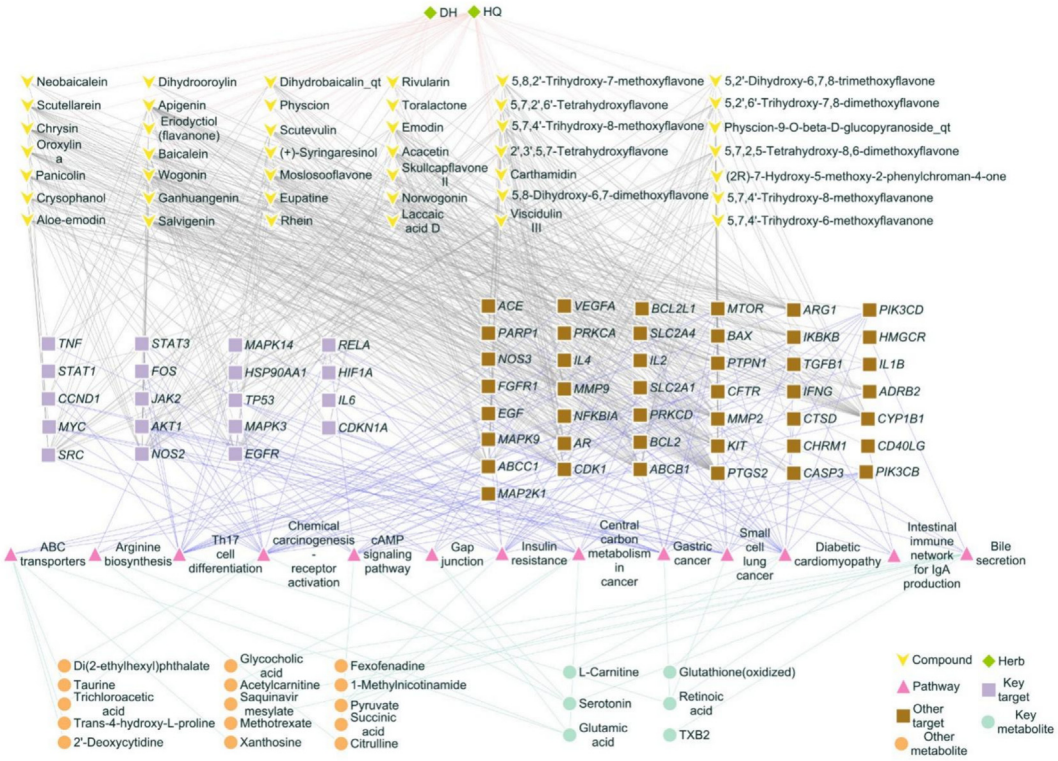

Fig. 12. "Pathway-metabolite-target-compound" network. Green diamond represents medicinal herb of QFP, yellow V-shape represents active compounds, purple square represents 19 key targets, brown square represents other targets, pink triangle represents 13 common pathways, light green ellipse represents significantly different metabolites (Fold change $\geq$ 2 or Fold change $\leq$ 1/2, $P < 0.05$, and VIP > 1), and orange ellipse represents other metabolites ($P < 0.05$ and VIP > 1).

was associated primarily of lipid metabolism, amino acid metabolism, and energy metabolism disturbances and that QFP partially recovered metabolic disturbances. In lung tissue, RSV-induced animal models displayed significantly elevated linoleic and oleic acid concentrations. The release of these free fatty acids is associated with an increased expression in IL-2, IL-4, and IL-6, with linoleic acid being the primary source of pro-inflammatory mediators (Dai et al., 2022). *In vitro* experiments on *ex vivo* rat airway smooth muscle tissues have also confirmed that linoleic acid and oleic acid can induce phosphorylation of the PI3K/AKT pathway (Matoba et al., 2018). Combined with KEGG pathway analysis, we speculated that these long-chain fatty acids were associated with the PI3K/AKT pathway activation and IL-6 overexpression in RSVP rats, causing aggravated inflammation. In addition to linoleic acid and oleic acid, arachidonic acid was involved in the immune response after RSV infection by regulating neutrophil adherence to infected cells. RSV immune complexes were shown to activate arachidonic acid metabolism. Apigenin has significantly inhibited cytochrome C oxidase (COX), preventing arachidonic acid's pro-inflammatory response from entering the cytoplasm (Makanjuola, Ogundaini, Ajonuma, & Dosunmu, 2018). In our research, the linoleic acid, oleic acid, and arachidonic acid levels in the model group were upsurged with the upregulated p-PI3K, p-AKT, and IL-6 compared with the normal group, indicating that fatty acid metabolism rep-

resented by linoleic acid metabolism indirectly induced severe inflammatory response. RSV infection mainly affects amino acid biosynthetic pathways, such as tryptophan, a critical molecule in inflammatory disease pathways. We analyzed common KEGG and metabolic pathways, ignoring pathways unrelated to RSVP pathogenesis. ABC transporters, arginine biosynthesis, cAMP signaling pathway, and Th17 cell differentiation were fundamental mechanisms suggesting therapeutic targets. After RSV infection, the inflammation from the airways and lungs aggregates neutrophils, leading to a pro-inflammatory cytokine environment typified by elevated IL-6 and the bias of immune response with raised Th2 and Th17 response as well as lessened Th1 response (Lambert, Sagfors, Openshaw, & Culley, 2014). Our previous experiments demonstrated that QFP can reverse the increase in Th17 cells caused by RSV infection and reduce inflammation (Wang, Zhang, Wang, Zhao, & Liu, 2023). ATP-binding cassette (ABC) transporters are HIF-1α-induced in Crohn's disease (Xie et al., 2018) but were significantly down-regulated in persistent lung inflammation after smoke exposure (Sonett et al., 2018). ABC transporters and cAMP play essential roles in energy metabolism and signal transduction, and we will verify their function in future studies. Interestingly, arginine, as one of the substrates for NOS2 synthesis (Schindler & Bogdan, 2001), was elevated in our RSVP rat model. Combined with our western blot results, it suggested that arginine may mediate the rise in NOS2. Our results demonstrated metabolic alterations in amino acids and nucleotides and energy metabolism-related pathways in RSVP rats, including *D*-glutamine and *D*-glutamate metabolism and alanine, aspartate and glutamate metabolism.

Despite the network pharmacological analysis, metabolomics, and *in vivo* experiments were used to investigate the pharmacologic mechanisms of QFP treatment in RSVP, our research still had several limitations. First, the advanced database online was used to predict transdermally absorption composition; however, our research needs detailed quantitative or qualitative data on the QFP, so we may have ignored the difference between the compound that plays the primary role and our prediction results. Secondly, further practical evidence *in vitro* is required to excavate the profound mechanism of QFP in RSVP treatment. The polymerase chain reaction (PCR) results of RSV-related genes were not determined in the lung and nose in our study because growing evidence reported that compared with viral titers, inflammatory response magnitude and congenital immunity are more relevant to the disease progression (Tahamtan, Samadizadeh, Rastegar, Nakstad, & Salimi, 2020; Thwaites et al., 2018). Thirdly, serum and lung tissue were mainly studied in our animal experiment, so further research in other potential organs is needed to reveal the biomarker changes. Finally, studies in specific tissues and organs are reasonable for investigating the general alterations of metabolism, such as the lungs and feces.

5. Conclusion

In summary, this integrative mode may submit an effective instrument for an initial apprehension of the mechanisms of TCMs. Analysis of pharmacological binding molecular docking in the online database showed that the active core components of QFP were apigenin, baicalein, and emodin. Moreover, in addition to the PI3K/AKT pathway and HIF-1 pathway as the decisive signaling pathways, IL-6, NOS2, EGFR and SRC were core targets for treating RSVP. Finally, our findings suggest that QFP may modulate linoleic acid metabolism, arachidonic acid metabolism, and some specific amino acid metabolisms as metabolic processes related to inflammation, immune regulation, and energy metabolism, thereby alleviating cytokine storm and inflammation. We will continue to validate these predictions experimentally to encourage broader utilization of QFP in clinical settings.

CRediT authorship contribution statement

Mengfei Yang: Data curation, Investigation, Methodology, Validation, Formal analysis, Software, Writing – original draft. **Xiuying Zhang:** Conceptualization, Funding acquisition, Investigation, Supervision, Writing – review & editing. **Qing Liu:** Data curation, Investigation. **Yongxue Wang:** Data curation, Investigation.

Declaration of Competing Interest

The authors declare that they have no known competing financial interests or personal relationships that could have appeared to influence the work reported in this paper.

Acknowledgments

This work was supported by the National Natural Science Foundation of China (No. 81973906).

Appendix A. Supplementary material

Supplementary material to this article can be found online at https://doi.org/10.1016/j.chmed.2024.07.007.

References

Alamri, M. A., ul Qamar, M. T., Afzal, O., Alabbas, A. B., Riadi, Y., & Alqahtani, S. M. (2021). Discovery of anti-MERS-CoV small covalent inhibitors through pharmacophore modeling, covalent docking and molecular dynamics simulation. *Journal of Molecular Liquids, 330*, 115699.

Bardou, P., Mariette, J., Escudié, F., Djemiel, C., & Klopp, C. (2014). jvenn: An interactive Venn diagram viewer. *BMC Bioinformatics, 15*(1), 293.

Belperio, J. A., Keane, M. P., Burdick, M. D., Londhe, V., Xue, Y. Y., Li, K., Phillips, R. J., & Strieter, R. M. (2002). Critical role for CXCR2 and CXCR2 ligands during the pathogenesis of ventilator-induced lung injury. *The Journal of Clinical Investigation, 110*(11), 1703–1716.

Besteman, S. B., Callaghan, A., Langedijk, A. C., Hennus, M. P., Meyaard, L., Mokry, M., Bont, L. J., & Calis, J. J. A. (2020). Transcriptome of airway neutrophils reveals an interferon response in life-threatening respiratory syncytial virus infection. *Clinical Immunology (Orlando, Fla.), 220*, 108593.

Bioinformatics (2021). https://www.bioinformatics.com.cn, 2022 (accessed 07 September 2022).

Bitko, V., Shulyayeva, O., Mazumder, B., Musiyenko, A., Ramaswamy, M., Look, D. C., & Barik, S. (2007). Nonstructural proteins of respiratory syncytial virus suppress premature apoptosis by an NF-kappaB-dependent, interferon-independent mechanism and facilitate virus growth. *Journal of Virology, 81*(4), 1786–1795.

Blunck, B. N., Aideyan, L., Ye, X., Avadhanula, V., Ferlic-Stark, L., Zechiedrich, L., Gilbert, B. E., & Piedra, P. A. (2021). A prospective surveillance study on the kinetics of the humoral immune response to the respiratory syncytial virus fusion protein in adults in Houston, Texas. *Vaccine, 39*(8), 1248–1256.

Britton, P. N., Hu, N., Saravanos, G., Shrapnel, J., Davis, J., Snelling, T., Dalby-Payne, J., Kesson, A. M., Wood, N., Macartney, K., McCullagh, C., & Lingam, R. (2020). COVID-19 public health measures and respiratory syncytial virus. *The Lancet Child & Adolescent Health, 4*(11), e42–e43.

Burley, S. K., Bhikadiya, C., Bi, C., Bittrich, S., Chen, L., Crichlow, G. V., ... Zhuravleva, M. (2021). RCSB Protein Data Bank: Powerful new tools for exploring 3D structures of biological macromolecules for basic and applied research and education in fundamental biology, biomedicine, biotechnology, bioengineering and energy sciences. *Nucleic Acids Research, 49*(D1), D437–D451.

Cheng, K., Wu, Z., Gao, B., & Xu, J. (2014). Analysis of influence of baicalin joint resveratrol retention enema on the TNF-α, SIgA, IL-2, IFN-γ of rats with respiratory syncytial virus infection. *Cell Biochemistry and Biophysics, 70*(2), 1305–1309.

Chow, E. J., Uyeki, T. M., & Chu, H. Y. (2022). The effects of the COVID-19 pandemic on community respiratory virus activity. *Nature Reviews. Microbiology, 21*(3), 195–210.

Consortium, U. (2023). UniProt: The universal protein knowledgebase in 2023. *Nucleic Acids Research, 51*(D1), D523–D531.

Currier, M. G., Lee, S., Stobart, C. C., Hotard, A. L., Villenave, R., Meng, J., ... Moore, M. L. (2016). EGFR interacts with the fusion protein of respiratory syncytial virus strain 2–20 and mediates infection and mucin expression. *PLoS Pathogens, 12*(5), e1005622.

Dai, P., Tang, Z., Qi, M., Liu, D., Bajinka, O., & Tan, Y. (2022). Dispersion and utilization of lipid droplets mediates respiratory syncytial virus-induced airway

hyperresponsiveness. *Pediatric Allergy and Immunology: Official Publication of the European Society of Pediatric Allergy and Immunology, 33*(1), e13651.
Daina, A., Michielin, O., & Zoete, V. (2017). SwissADME: A free web tool to evaluate pharmacokinetics, drug-likeness and medicinal chemistry friendliness of small molecules. *Scientific Reports, 7*, 42717.
Daina, A., Michielin, O., & Zoete, V. (2019). SwissTargetPrediction: Updated data and new features for efficient prediction of protein targets of small molecules. *Nucleic Acids Research, 47*(W1), W357–W364.
Damasio, G. A. C., Pereira, L. A., Moreira, S. D. R., Duarte dos Santos, C. N., Dalla-Costa, L. M., & Raboni, S. M. (2015). Does virus-bacteria coinfection increase the clinical severity of acute respiratory infection? *Journal of Medical Virology, 87*(9), 1456–1461.
de Steenhuijsen Piters, W. A. A., Heinonen, S., Hasrat, R., Bunsow, E., Smith, B., Suarez-Arrabal, M. C., ... Mejias, A. (2016). Nasopharyngeal microbiota, host transcriptome, and disease severity in children with respiratory syncytial virus infection. *American Journal of Respiratory and Critical Care Medicine, 194*(9), 1104–1115.
Edgar, R., Domrachev, M., & Lash, A. E. (2002). Gene Expression Omnibus: NCBI gene expression and hybridization array data repository. *Nucleic Acids Research, 30*(1), 207–210.
Groskreutz, D. J., Monick, M. M., Yarovinsky, T. O., Powers, L. S., Quelle, D. E., Varga, S. M., ... Hunninghake, G. W. (2007). Respiratory syncytial virus decreases p53 protein to prolong survival of airway epithelial cells. *The Journal of Immunology, 179*(5), 2741–2747.
Habibi, M. S., Jozwik, A., Makris, S., Dunning, J., Paras, A., DeVincenzo, J. P., ... Chiu, C. (2015). Impaired antibody-mediated protection and defective IgA B-cell memory in experimental infection of adults with respiratory syncytial virus. *American Journal of Respiratory and Critical Care Medicine, 191*(9), 1040–1049.
Hao, O., Wang, X., Liu, S., Shao, R., & Xie, B. (2016). Effect of Fuxiong Cream on expressions of JNK and MKK4 in lung tissue of rats with influenza A virus pneumonia. *Chinese Journal of Experimental Traditional Medical Formulae, 22*(23), 111–115.
Jain, H., Schweitzer, J. W., & Justice, N. A. (2023). Respiratory syncytial virus infection. *StatPearls [Internet]*. StatPearls Publishing.
Jones, S. A., & Jenkins, B. J. (2018). Recent insights into targeting the IL-6 cytokine family in inflammatory diseases and cancer. *Nature Reviews Immunology, 18*(12), 773–789.
Kalinowski, A., Galen, B. T., Ueki, I. F., Sun, Y., Mulenos, A., Osafo-Addo, A., ... Koff, J. L. (2018). Respiratory syncytial virus activates epidermal growth factor receptor to suppress interferon regulatory factor 1-dependent interferon-lambda and antiviral defense in airway epithelium. *Mucosal Immunology, 11*(3), 958–967.
Kim, S., Chen, J., Cheng, T., Gindulyte, A., He, J., He, S., ... Bolton, E. E. (2019). PubChem 2019 update: Improved access to chemical data. *Nucleic Acids Research, 47*(D1), D1102–D1109.
Kui, F., Gu, W., Gao, F., Niu, Y., Li, W., Zhang, Y., ... Du, G. (2021). Research on effect and mechanism of Xuefu Zhuyu Decoction on CHD based on meta-analysis and network pharmacology. *Evidence-based Complementary and Alternative Medicine: ECAM, 2021*, 9473531.
Lambert, L., Sagfors, A. M., Openshaw, P. J. M., & Culley, F. J. (2014). Immunity to RSV in early-life. *Frontiers in Immunology, 5*, 466.
Li, L., Xu, W., Luo, Y., Lao, C., Tong, X., Du, J., ... Li, J. (2022). Aloe polymeric acemannan inhibits the cytokine storm in mouse pneumonia models by modulating macrophage metabolism. *Carbohydrate Polymers, 297*, 120032.
Lingemann, M., McCarty, T., Liu, X., Buchholz, U. J., Surman, S., Martin, S. E., ... Munir, S. (2019). The alpha-1 subunit of the Na^+,K^+-ATPase (ATP1A1) is required for macropinocytic entry of respiratory syncytial virus (RSV) in human respiratory epithelial cells. *PLoS Pathogens, 15*(8), e1007963.
Liu, Z., Ma, N., Zhong, Y., & Yang, Z. Q. (2015). Antiviral effect of emodin from *Rheum palmatum* against coxsakievirus B5 and human respiratory syncytial virus *in vitro*. *Journal of Huazhong University of Science and Technology, 35*(6), 916–922.
Makanjuola, S. B. L., Ogundaini, A. O., Ajonuma, L. C., & Dosunmu, A. (2018). Apigenin and apigeninidin isolates from the *Sorghum bicolor* leaf targets inflammation via cyclo-oxygenase-2 and prostaglandin-E2 blockade. *International Journal of Rheumatic Diseases, 21*(8), 1487–1495.
Manning, B. D., & Cantley, L. C. (2007). AKT/PKB signaling: Navigating downstream. *Cell, 129*(7), 1261–1274.
Mannová, P., & Beretta, L. (2005). Activation of the N-Ras-PI3K-Akt-mTOR pathway by hepatitis C virus: Control of cell survival and viral replication. *Journal of Virology, 79*(14), 8742–8749.
Matoba, A., Matsuyama, N., Shibata, S., Masaki, E., Emala, C. W., & Mizuta, K. (2018). The free fatty acid receptor 1 promotes airway smooth muscle cell proliferation through MEK/ERK and PI3K/Akt signaling pathways. *American Journal of Physiology-Lung Cellular and Molecular Physiology, 314*(3), L333–L348.
Mayer, A. K., Muehmer, M., Mages, J., Gueinzius, K., Hess, C., Heeg, K., ... Dalpke, A. H. (2007). Differential recognition of TLR-dependent microbial ligands in human bronchial epithelial cells. *The Journal of Immunology, 178*(5), 3134–3142.
McCready, C., Haider, S., Little, F., Nicol, M. P., Workman, L., Gray, D. M., ... Zar, H. J. (2023). Early childhood wheezing phenotypes and determinants in a South African birth cohort: Longitudinal analysis of the Drakenstein Child Health Study. *The Lancet Child & Adolescent Health, 7*(2), 127–135.
McNamara, P. S., Flanagan, B. F., Selby, A. M., Hart, C. A., & Smyth, R. L. (2004). Pro- and anti-inflammatory responses in respiratory syncytial virus bronchiolitis. *The European Respiratory Journal, 23*(1), 106–112.
Mejias, A., Dimo, B., Suarez, N. M., Garcia, C., Suarez-Arrabal, M. C., Jartti, T., ... Ramilo, O. (2013). Whole blood gene expression profiles to assess pathogenesis and disease severity in infants with respiratory syncytial virus infection. *PLoS Medicine, 10*(11), e1001549.
MetaboAnalyst (2009). http://www.metaboanalyst.ca/, 2022 (accessed 01 December 2022).
Morris, D. R., Qu, Y., Agrawal, A., Garofalo, R. P., & Casola, A. (2020). HIF-1α modulates core metabolism and virus replication in primary airway epithelial cells infected with respiratory syncytial virus. *Viruses, 12*(10), 1088.
Morris, G. M., Huey, R., Lindstrom, W., Sanner, M. F., Belew, R. K., Goodsell, D. S., & Olson, A. J. (2009). AutoDock4 and AutoDockTools4: Automated docking with selective receptor flexibility. *Journal of Computational Chemistry, 30*(16), 2785–2791.
Naik, A., Kalia, Y. N., & Guy, R. H. (2000). Transdermal drug delivery: Overcoming the skin's barrier function. *Pharmaceutical Science & Technology Today, 3*(9), 318–326.
Nair, H., Nokes, D. J., Gessner, B. D., Dherani, M., Madhi, S. A., Singleton, R. J., ... Campbell, H. (2010). Global burden of acute lower respiratory infections due to respiratory syncytial virus in young children: A systematic review and meta-analysis. *Lancet (London, England), 375*(9725), 1545–1555.
Openshaw, P. J. M., Chiu, C., Culley, F. J., & Johansson, C. (2017). Protective and harmful immunity to RSV infection. *Annual Review of Immunology, 35*, 501–532.
Perchiazzi, G., Larina, A., Hansen, T., Frithiof, R., Hultström, M., Lipcsey, M., & Pellegrini, M. (2022). Chest dual-energy CT to assess the effects of steroids on lung function in severe COVID-19 patients. *Critical Care (London, England), 26*(1), 328.
Phipps, S., Lam, C. E., Mahalingam, S., Newhouse, M., Ramirez, R., Rosenberg, H. F., ... Matthaei, K. I. (2007). Eosinophils contribute to innate antiviral immunity and promote clearance of respiratory syncytial virus. *Blood, 110*(5), 1578–1586.
Pu, Z., Shen, C., Zhang, W., Xie, H., & Wang, W. (2022). Avenanthramide C from oats protects pyroptosis through dependent ROS-induced mitochondrial damage by PI3K ubiquitination and phosphorylation in pediatric pneumonia. *Journal of Agricultural and Food Chemistry, 70*(7), 2339–2353.
Punnoose, A. R., & Golub, R. M. (2012). Respiratory syncytial virus bronchiolitis. *The Journal of the American Medical Association, 307*(2), 213.
Ru, J., Li, P., Wang, J., Zhou, W., Li, B., Huang, C., ... Yang, L. (2014). TCMSP: A database of systems pharmacology for drug discovery from herbal medicines. *Journal of Cheminformatics, 6*, 13.
Schindler, H., & Bogdan, C. (2001). NO as a signaling molecule: Effects on kinases. *International Immunopharmacology, 1*(8), 1443–1455.
Schrödinger, L., DeLano, W. (2020). *PyMOL*. Retrieved from http://www.pymol.orgpymol.
Seki, E., Yoshizumi, M., Tanaka, R., Ryo, A., Ishioka, T., Tsukagoshi, H., ... Kimura, H. (2013). Cytokine profiles, signalling pathways and effects of fluticasone propionate in respiratory syncytial virus-infected human foetal lung fibroblasts. *Cell Biology International, 37*(4), 326–339.
Shannon, P., Markiel, A., Ozier, O., Baliga, N. S., Wang, J. T., Ramage, D., ... Ideker, T. (2003). Cytoscape: A software environment for integrated models of biomolecular interaction networks. *Genome Research, 13*(11), 2498–2504.
Shi, H., Ren, K., Lv, B., Zhang, W., Zhao, Y., Tan, R. X., & Li, E. (2016). Baicalin from *Scutellaria baicalensis* blocks respiratory syncytial virus (RSV) infection and reduces inflammatory cell infiltration and lung injury in mice. *Scientific Reports, 6*, 35851.
Sonett, J., Goldklang, M., Sklepkiewicz, P., Gerber, A., Trischler, J., Zelonina, T., ... D'Armiento, J. (2018). A critical role for ABC transporters in persistent lung inflammation in the development of emphysema after smoke exposure. *FASEB Journal: Official Publication of the Federation of American Societies for Experimental Biology, 32*(12), fj201701381.
Stelzer, G., Rosen, N., Plaschkes, I., Zimmerman, S., Twik, M., Fishilevich, S., ... Lancet, D. (2016). The GeneCards suite: From gene data mining to disease genome sequence analyses. *Current Protocols in Bioinformatics, 54*(1), 1–30.
Szklarczyk, D., Gable, A. L., Nastou, K. C., Lyon, D., Kirsch, R., Pyysalo, S., ... von Mering, C. (2021). The STRING database in 2021: Customizable protein-protein networks, and functional characterization of user-uploaded gene/measurement sets. *Nucleic Acids Research, 49*(D1), D605–D612.
Tahamtan, A., Besteman, S., Samadizadeh, S., Rastegar, M., Bont, L., & Salimi, V. (2021). Neutrophils in respiratory syncytial virus infection: From harmful effects to therapeutic opportunities. *British Journal of Pharmacology, 178*(3), 515–530.
Tahamtan, A., Samadizadeh, S., Rastegar, M., Nakstad, B., & Salimi, V. (2020). Respiratory syncytial virus infection: Why does disease severity vary among individuals? *Expert Review of Respiratory Medicine, 14*(4), 415–423.
Tang, Y., Li, M., Wang, J., Pan, Y., & Wu, F. X. (2015). CytoNCA: A cytoscape plugin for centrality analysis and evaluation of protein interaction networks. *Biosystems, 127*, 67–72.
Taylor, C. T., & Colgan, S. P. (2017). Regulation of immunity and inflammation by hypoxia in immunological niches. *Nature Reviews Immunology, 17*(12), 774–785.
Thomas, K. W., Monick, M. M., Staber, J. M., Yarovinsky, T., Carter, A. B., & Hunninghake, G. W. (2002). Respiratory syncytial virus inhibits apoptosis and induces NF-kappa B activity through a phosphatidylinositol 3-kinase-dependent pathway. *The Journal of Biological Chemistry, 277*(1), 492–501.
Thwaites, R. S., Coates, M., Ito, K., Ghazaly, M., Feather, C., Abdulla, F., ... Openshaw, P. (2018). Reduced nasal viral load and IFN responses in infants with respiratory syncytial virus bronchiolitis and respiratory failure. *American Journal of Respiratory and Critical Care Medicine, 198*(8), 1074–1084.
Tsutsumi, H., Takeuchi, R., Ohsaki, M., Seki, K., & Chiba, S. (1999). Respiratory syncytial virus infection of human respiratory epithelial cells enhances

inducible nitric oxide synthase gene expression. *Journal of Leukocyte Biology, 66*(1), 99–104.
Ujiie, M., Tsuzuki, S., Nakamoto, T., & Iwamoto, N. (2021). Resurgence of respiratory syncytial virus infections during COVID-19 pandemic, Tokyo, Japan. *Emerging Infectious Diseases, 27*(11), 2969–2970.
Van Royen, T., Rossey, I., Sedeyn, K., Schepens, B., & Saelens, X. (2022). How RSV proteins join forces to overcome the host innate immune response. *Viruses, 14*(2), 419.
Vargas, J. E., Puga, R., de Faria Poloni, J., Saraiva Macedo Timmers, L. F., Porto, B. N., ... Tetelbom Stein, R. (2015). A network flow approach to predict protein targets and flavonoid backbones to treat respiratory syncytial virus infection. *BioMed Research International, 2015*, 301635.
Ventre, K., & Randolph, A. G. (2007). Ribavirin for respiratory syncytial virus infection of the lower respiratory tract in infants and young children. *Cochrane Database of Systematic Reviews, 1*, CD000181.
Wang, X., (2015). *Study of the regulatory effect of Qingfei Tongluo plaster on the regulation of IL-6 and TNF-α in pneumonia models of young rats with RSV infection*. Liaoning University of Traditional Chinese Medicine. Thesis of Master Degree.
Wang, Y., Chen, M., Zhang, J., Zhang, X. L., Huang, X. J., Wu, X., Zhang, Q. W., Li, Y. L., & Ye, W. C. (2012). Flavone *C*-glycosides from the leaves of *Lophatherum gracile* and their *in vitro* antiviral activity. *Planta Medica, 78*(1), 46–51.
Wang, Y., Zhang, X., Wang, X., Zhao, H., & Liu, Q. (2023). Effects of Qingfei Tongluo Fuxiong Recipe on Treg/Th17 and related cytokines in alveolar lavage fluid of young rats with RSV induced lung injury. *Liaoning Journal of Traditional Chinese Medicine*, 1–8.
Wei, W., Bai, X., Wang, X., Wu, Z., Wang, W., Zhao, X., ... Zhang, Z. (2013). Based on the clinical research integration platform, a prospective study on the impact of TCM internal and external combined treatment on the main symptom of childhood pneumonia. *Chinese Pediatrics of Integrated Traditional and Western Medicine, 5*(4), 323–325.
Wildenbeest, J. G., Billard, M. N., Zuurbier, R. P., Korsten, K., Langedijk, A. C., van de Ven, P. M., ... Bont, L. J. (2022). The burden of respiratory syncytial virus in healthy term-born infants in Europe: A prospective birth cohort study. *The Lancet Respiratory Medicine, 11*(4), 341–353.
Wishart, D. S., Feunang, Y. D., Guo, A. C., Lo, E. J., Marcu, A., Grant, J. R., ... Wilson, M. (2018). DrugBank 5.0: A major update to the DrugBank database for 2018. *Nucleic Acids Research, 46*(D1), D1074–D1082.
Xie, A., Robles, R. J., Mukherjee, S., Zhang, H., Feldbrügge, L., Csizmadia, E., ... Longhi, M. S. (2018). HIF-1α-induced xenobiotic transporters promote Th17 responses in Crohn's disease. *Journal of Autoimmunity, 94*, 122–133.
Zeng, Z. (2014). *Syndrome type of three Chengqi Decoction based on data mining.* Beijing University of Chinese Medicine. Thesis of Master Degree.
Zhang, X. (2016). *Based on the theory of cortical chords, the multi-target mechanism of Qingfei Tongluo plater on RSV pneumonia in young rats was discussed*. Liaoning University of Traditional Chinese Medicine. Thesis of Master Degree.
Zhou, Y., Zhou, B., Pache, L., Chang, M., Khodabakhshi, A. H., Tanaseichuk, O., ... Chanda, S. K. (2019). Metascape provides a biologist-oriented resource for the analysis of systems-level datasets. *Nature Communications, 10*(1), 1523.
Zhang, X., Wang, X., Liu, X., & Wang, Y. (2016). Influence of Qigfei Tongluo Paste on MAPK signal pathway in lung tissue of respiratory syncytical virus pneumonia in rats. *Chinese Archives of Traditional Chinese Medicine, 34*(7), 1588–1590.
Zhang, X., Wang, X., Shang, Y., Cui, Z., Huang, Y., Wang, Y., ... Zhao, Y. (2017). Clinical observation on treatment of 460 community-acquired pneumonia cases in children with Qing-Fei Tong-Luo ointment. *World Science Technology-Modernization of Traditional Chinese Medicine, 19*(12), 2054–2057.
Zhang, X., Wang, X., & Song, N. (2016). Influence of Qingfeitongluo-pastesn and its different disassembled formula on virus load in lung tissue of respiratory syncytial virus pneumonia in rats. *Lishizhen Medicine and Materia Medica Research, 27*(6), 1307–1309.
Zhang, X., Wang, X., & Yan, F. (2017). Influence of Qingfeitongluo-pastes on T-lymphocyte subsets and related cytokines in peripheral blood of rats with respiratory syncytial virus pneumonia. *Modern Journal of Integrated Traditional Chinese and Western Medicine, 26*(31), 3421–3424.
Zhou, Y., Zhou, B., Pache, L., Chang, M., Khodabakhshi, A. H., Tanaseichuk, O., ... Chanda, S. K. (2019). Metascape provides a biologist-oriented resource for the analysis of systems-level datasets. *Nature Communications, 10*(1), 1523.
Zhang, X., Wang, X., Liu, X., & Wang, Y. (2016). Influence of Qigfei Tongluo Paste on MAPK signal pathway in lung tissue of respiratory syncytical virus pneumonia in rats. *Chinese Archives of Traditional Chinese Medicine, 34*(7), 1588–1590.
Zhang, X., Wang, X., Shang, Y., Cui, Z., Huang, Y., Wang, Y., ... Zhao, Y. (2017). Clinical observation on treatment of 460 community-acquired pneumonia cases in children with Qing-Fei Tong-Luo ointment. *World Science Technology-Modernization of Traditional Chinese Medicine, 19*(12), 2054–2057.
Zhang, X., Wang, X., & Song, N. (2016). Influence of Qingfeitongluo-pastesn and its different disassembled formula on virus load in lung tissue of respiratory syncytial virus pneumonia in rats. *Lishizhen Medicine and Materia Medica Research, 27*(6), 1307–1309.
Zhang, X., Wang, X., & Yan, F. (2017). Influence of Qingfeitongluo-pastes on T-lymphocyte subsets and related cytokines in peripheral blood of rats with respiratory syncytial virus pneumonia. *Modern Journal of Integrated Traditional Chinese and Western Medicine, 26*(31), 3421–3424.
Zhou, F., & Feng, Y. (2023). Homogenization study of traditional Chinese medicine compound preparation and discussion on medicinal substances in preparation. *Chinese Traditional and Herbal Drugs, 54*(8), 2357–2364.